

What influences the lifespan of a vortex?

M4R Project

Author: Frederica Melbourne

CID: 01068192

Supervisor: Dr Igor Shevchenko

11th June 2019

This is my own unaided work unless stated otherwise.

Abstract

This focus of this project is the study of mesoscale vortices in a fine-grid ocean simulation derived from a three-layer quasi-geostrophic model with wind-forcing and bottom viscosity terms. The potential vorticity anomaly data was appropriate for representing a plane approximation of the Gulf Stream. A tracking algorithm is developed to follow the vortices through time, and then the characteristics of the population (including differences between the cyclones and anticyclones) and of the long-lived vortices in particular are investigated, as well as the contrasts between cyclones and anticyclones. Finally, linear stability analysis of vortices in contrasting environments is performed.

Contents

1	Introduction	4
2	Fundamental Definitions	5
3	The Governing Equations	6
3.1	The Shallow Water Equations	6
3.2	The Quasi-Geostrophic Equations	7
3.2.1	Non-Dimensionalising the Equations	7
3.2.2	Asymptotics	8
3.2.3	The 3-Layer QG Equations	10
4	Data Assimilation	11
5	Obtaining and Sorting the Vortices	13
5.1	Vortex Extraction Algorithm	13
5.2	Preparing the PV Anomaly Field	13
5.3	Obtaining the Vortices	15
5.4	Sorting the Vortices	16
6	Tracking the Vortices	18
7	Results	22
7.1	Characteristics of the Population	22
7.1.1	Energies and Energy Densities	26
7.2	Effects of Characteristics on Vortex Lifespan	28
7.3	Comparison of Cyclonic and Anticyclonic Vortices	32
7.3.1	Relationship Between Characteristics	34
7.4	Analysis of Long-Lived Vortices	36
7.5	Stability Analysis	40
8	Conclusion	42
9	Appendix	44
9.1	Obtaining the Vortices	44
9.2	Sorting the Vortices	45
9.3	Tracking Algorithm	46
9.4	Properties of the Vortices	49
9.4.1	Lifespans	49
9.4.2	Terminations and Formations	50
9.4.3	Areas	51
9.4.4	Speeds and Distances	51
9.4.5	Energies and Energy Densities	52
9.5	Cyclonic and Anticyclonic Vortices	55
9.6	Other Functions	57

1 Introduction

Vortices are described in [Green, 1995] as highly conspicuous structures in any fluid flow. There is no single definition of a vortex- it can be thought of as a region of high vorticity compared to the flow surrounding it. Since the vorticity equation can be obtained from a momentum equation by taking the curl, all information in the velocity field is contained also in the vorticity field. The fact that vortices may be characterized by this simple property means that their study is tractable.

The vortices studied in this project are the mesoscale vortices embedded in a three-layer Gulf Stream simulation, which is described in [Carton, 2001] as having motions with length scales of the order of a hundred kilometres. In general, these vortices form as a result of the instabilities of the Gulf Stream which grow downstream and lead to the detachment of rings. It tends to be that anticyclonic vortices (those with negative vorticity) are found to the north of the jet, trapping warm water from the south, and that colder, larger cyclonic vortices are found to the south.

These vortices trap the water mass inside their boundary at formation, with only slight mixing with the surrounding water at the vortex boundary. They are known to be energetic, long-lived and to travel long distances. Thus the vortices play an important role in ocean thermodynamics, since they carry fixed masses of water across the ocean. Hence also their study is necessary to increase understanding of the global climate system, of which the ocean is one of the most fundamental and least understood components, as noted in [Shevchenko and Berloff, 2015].

It is remarked in [Carton, 2001] that the potential vorticity is an ideal quantity to choose to characterize oceanic vortices. This is the crucial quantity involved in the quasi-geostrophic model, which combines both the forces arising due to the rotation of the Earth and due to the rotation of the vortex itself. This model also allows for the ocean to be discretized as layers of constant density, which makes the problem of ocean simulation tractable. Therefore within this project, we study the potential vorticity field generated from a QG model (through CABARET), in a simulation of the Gulf Stream region.

The study of the mesoscale vortices in this flow (in particular with the aforementioned data) is in its early stages, and hence this project is highly exploratory in nature. The goal is to assess the connections between the various derived properties of the vortices, in order to gain a better understanding of them. We would like to determine the differences between the cyclonic and anticyclonic vortices, and also to examine the longest-lived vortices in detail to see if there are particular conditions which give rise to a vortex being able to survive. We hope also to examine differences in the linear stability of the vortices in different environments.

2 Fundamental Definitions

Material Derivative

$$\frac{D}{Dt} = \frac{\partial}{\partial t} + \underline{u} \cdot \nabla = \frac{\partial}{\partial t} + u \frac{\partial}{\partial x} + v \frac{\partial}{\partial y} + w \frac{\partial}{\partial z}$$

Stream Function This is a scalar field which is constant along the streamlines of the flow. We require only the (simpler) two-dimensional case:

$$\psi = \psi(x, y), \quad \frac{\partial \psi}{\partial y} = u, \quad -\frac{\partial \psi}{\partial x} = v$$

Relative Vorticity This quantity describes the local rotation of fluid particles, and may be expressed in terms of the stream function:

$$\zeta = \nabla \times \underline{u} = \frac{\partial v}{\partial y} - \frac{\partial u}{\partial x} = -\nabla^2 \psi$$

Boussinesq Approximation

It is stated in [Berloff, 2018] that under the Boussinesq approximation the variation of fluid density ρ is small. We can write $\rho = \rho_0 + \bar{\rho}(z) + \rho'(x, y, t)$, where the dynamic anomaly $\rho' \ll \rho_0$, and $\bar{\rho}z$ may be neglected but not its derivative. x

Hydrostatic Approximation

Here it is assumed that the gravity force is balanced by the vertical pressure gradient:

$$\frac{\partial p}{\partial z} = -\rho g$$

This approximation results in vertical acceleration $\frac{Dw}{Dt}$ being negligible. Furthermore, the horizontal accelerations become independent of z, so that the flow can be regarded as two-dimensional (\underline{u} - (u,v)). [Berloff, 2018]

The hydrostatic-Boussinesq approximation is a common choice of assumptions for the analysis of oceanic flows, leading to a reduced set of equations which require lower computational cost.

Coriolis Parameter

The Coriolis effect refers to the apparent force which deflects fluid particles due to the rotation of the Earth. In this project, it is sometimes represented by $f\hat{k}$. The parameter f can be given by $2\Omega \sin(\theta)$, (for rotation rate Ω and latitude θ), but we use the β -plane approximation $f = f_0 + \beta y$.

3 The Governing Equations

We now proceed to give a brief derivation of the quasi-geostrophic equations as in [Vallis, 2006]. This system of equations is a commonly used ocean model from which the majority of the raw data used in this paper is generated. We begin with the simpler case of the shallow water equations.

3.1 The Shallow Water Equations

These simple equations describe a thin layer of fluid, bounded below by a fixed topography and with a free surface above, for which the hydrostatic and Bousinnesq approximations may be invoked. Specifically, the force due to gravity is balanced by a vertical pressure force, and density is treated as constant.

The single layer equations are given by the two momentum equations and the continuity equation:

$$\begin{aligned}\frac{Du}{Dt} - fv &= -g \frac{\partial \eta}{\partial x} \\ \frac{Dv}{Dt} + fu &= -g \frac{\partial \eta}{\partial y} \\ \frac{\partial h}{\partial t} + h \nabla \cdot \underline{u} &= 0\end{aligned}$$

The notation used here is described in the below table:

Notation	Quantity
$\eta(x, y, t)$	Height of the free surface
$\eta_b(x, y, t)$	Height of the bottom topography
$h(x, y, t) = \eta - \eta_b$	Layer thickness
$\underline{u} = (u, v)$	Two-dimensional velocity
f	Coriolis parameter
g	Gravitational constant

The equations may be generalised to a three-layer model, such as the isopycnic ocean model that is used in this project. The main difference is that density is assumed to be constant within each layer but may jump discontinuously across layers.

The momentum equation in the n th layer takes the form:

$$\frac{D\underline{u}_n}{Dt} + \underline{f} \times \underline{u}_n = -\frac{1}{\rho_n} \nabla p_n, \quad n = 1, 2, 3$$

The equation is dependent on the pressure in the n th layer, which is given by:

$$p_n = p_1 \sum_{i=0}^{n-1} g'_i \eta_i \quad n = 1, 2, 3$$

This in turn depends on the reduced gravity:

$$g'_i = g \frac{\rho_{i+1} - \rho_i}{\rho_i}, \quad i = 1, 2$$

$$g'_0 = g$$

Finally, the continuity equation for the thickness of each layer is unchanged from the single-layer case:

$$\frac{Dh_n}{Dt} + h_n \nabla \cdot \underline{u}_n, \quad n = 1, 2, 3$$

Shallow Water Potential Vorticity

An important quantity in the course of this project is the potential vorticity. For the single-layer shallow water model, this is the materially-invariant quantity

$$Q = \frac{\zeta + f}{h}, \quad \frac{DQ}{Dt} = 0$$

where $\zeta(x, y, t)$ is the relative vorticity.

3.2 The Quasi-Geostrophic Equations

The shallow water equations described in the last equation may be simplified to obtain a set of quasi-geostrophic equations which describe fluid motion on a horizontal scale similar to that at which mesoscale vortex motion takes place. It is the most commonly used ocean model for analysing activity at this scale, and is the model from which the data analysed in this project was generated.

3.2.1 Non-Dimensionalising the Equations

The first step in deriving these equations is to obtain a nondimensional form of the shallow water single-layer equations. We define the following scales:

$$(u, v) = U(\hat{u}, \hat{v}) \quad (x, y) = L(\hat{x}, \hat{y}) \quad t = \frac{L}{U} \hat{t}$$

and scale the change in the free surface, $\Delta\eta$, by A .

Thus the terms in the in the single-layer shallow water momentum equation have scales $\frac{U^2}{L}$, $\frac{U^2}{L}$, fU and $\frac{gA}{L}$ respectively. If we choose the last two terms to be balanced, we have the geostrophic balance, i.e. the Coriolis term is balanced by the pressure force:

$$\underline{f} \times \underline{u} \approx -g \nabla \eta$$

$$fU \quad \frac{gA}{L}$$

This implies $A = \frac{fUL}{g}$. Here we need a definition which will be used later for asymptotic analysis of the equations.

Rossby Number

$Ro = \frac{U}{fL}$ is the ratio of advective and rotational terms. For oceanic flows it is generally small, i.e. $Ro \ll 1$.

Thus we can write the scale for $\Delta\eta$ as $A = Ro H \frac{L}{L_d^2}$, where, $L_d = \frac{\sqrt{gH}}{f}$ is the deformation radius of the fluid, and H is the mean thickness of the layer. Therefore we obtain the non-dimensional variables for both $\Delta\eta$ and $\eta = H + \Delta\eta$:

$$\eta = H(1 + Ro \frac{L^2}{L_d^2} \hat{\eta}) \quad \Delta\eta = Ro \frac{L^2}{L_d^2} H \hat{\eta}.$$

Define the parameter $F = (\frac{L}{L_d})^2$.

We can now use the scalings for velocity, lengths, time and the height of the free surface and its deviation from the mean thickness H , to obtain the non-dimensional forms of the shallow water equations:

$$\begin{aligned} Ro \left(\frac{\partial \hat{u}}{\partial \hat{t}} (\hat{u} \cdot \nabla) \hat{u} + \underline{f} \times \hat{u} \right) &= -\nabla \hat{\eta} \\ Ro F \frac{D\hat{\eta}}{D\hat{t}} + (1 + Ro F \hat{\eta}) \nabla \cdot \hat{u} &= 0 \end{aligned}$$

3.2.2 Asymptotics

We now make use of a specific choice of assumptions and use the corresponding asymptotic expansions of the variables to obtain a closed system of quasi-geostrophic equations, which will be used to generate the data which is analysed in this project.

We assume that Ro is small (very reasonable for mesoscale oceanic flows) and that variations in the Coriolis parameter are small. Then we proceed to expand in terms of Ro :

$$\begin{aligned} \hat{u} &= \hat{u}_0 + Ro \hat{u}_1 + Ro^2 \hat{u}_2 + \dots \\ \hat{v} &= \hat{v}_0 + Ro \hat{v}_1 + Ro^2 \hat{v}_2 + \dots \\ \hat{\eta} &= \hat{\eta}_0 + Ro \hat{\eta}_1 + Ro^2 \hat{\eta}_2 + \dots \end{aligned}$$

Also, to ensure that the variations in f are small, we let $\beta = \frac{U}{L^2} \hat{f}$, so that $\hat{f} = \hat{f}_0 + Ro \hat{\beta} \hat{y}$, is the non-dimensional form of f .

From here, we substitute the expansions into the non-dimensionalised shallow water equations and equate the powers of Ro .

Continuity Equation

- At zeroth order, we have simply that $\nabla \cdot \underline{u}_0 = 0$.

- At first order, we get:

$$F \frac{\partial \hat{\eta}_0}{\partial \hat{t}} + F \hat{u}_0 \cdot \nabla \hat{\eta}_0 + \nabla \cdot \hat{u}_1 = 0$$

Momentum Equations

- At zeroth order, we have that

$$\hat{f}_0 \hat{u}_0 = - \frac{\partial \hat{\eta}_0}{\partial \hat{y}}, \quad \hat{f}_0 \hat{v}_0 = \frac{\partial \hat{\eta}_0}{\partial \hat{x}} \quad \Rightarrow \nabla \cdot \underline{u}_0 = 0$$

- At first order:

$$\frac{\partial \hat{u}_0}{\partial \hat{t}} + (\hat{u}_0 \cdot \nabla) \underline{u}_0 + (\hat{\beta} \hat{y} \hat{k} \times \hat{u}_0) + (f_0 \hat{k} \times \hat{u}_1) = -\nabla \eta_0$$

By taking the curl of the momentum equations a first order, making use of the vector identity:

$$\nabla \times (A \times B) = A \nabla \cdot B - B \nabla \cdot A + (B \cdot \nabla A) - (A \cdot \nabla B)$$

and the fact that the divergence of the velocity is zero at first order, we get that:

$$\frac{\partial \hat{\zeta}_0}{\partial \hat{t}} + (\hat{u}_0 \cdot \nabla) (\hat{\zeta}_0 + \hat{\beta} \hat{y}) = -\hat{f}_0 \nabla \cdot \hat{u}_1$$

By equating this with the continuity equation at first order, we arrive at:

$$\frac{D}{D \hat{t}} (\hat{\zeta}_0 + \hat{\beta} \hat{y} - F \hat{f}_0 \hat{\eta}_0) = 0$$

Now we notice that from the momentum equations at zeroth order, it is possible to define a stream function by $\hat{\psi}_0 = \frac{\hat{\eta}_0}{\hat{f}_0}$, so:

$$\frac{D}{D \hat{t}} (\nabla^2 \hat{\psi}_0 + \hat{\beta} \hat{y} - f_0^2 F \hat{\psi}_0) = 0$$

We can drop the non-dimensional variables now, so that we have finally arrived at the expression for the quasi-geostrophic potential vorticity:

$$q = \nabla^2 \psi + \beta y - \frac{\psi}{L_d^2} \quad \frac{Dq}{Dt} = 0$$

3.2.3 The 3-Layer QG Equations

Just as for the shallow water equations, it is possible to arrive at a three-layer system for the quasi-geostrophic equations, which is applicable to our isopycnic model of the ocean involving three layers stacked on top of each other. This is done by defining stream functions in each layer, in terms of reduced gravities and layer thicknesses. As before, the density is taken to be constant in each layer, but jumps discontinuously between layers.

The 3-layer equations are as follows:

$$\begin{aligned} q_1 &= \beta y + \nabla^2 \psi_1 + \frac{f_0^2}{H_1} \left(\frac{\psi_2 - \psi_1}{g'_1} \right) - \frac{f_0^2}{g H_1 \psi_1} \\ q_2 &= \beta y + \nabla^2 \psi_2 + \frac{f_0^2}{H_2} \left(\frac{\psi_1 - \psi_2}{g'_1} - \frac{\psi_2 - \psi_3}{g'_2} \right) \\ q_3 &= \beta y + \nabla^2 \psi_3 + \frac{f_0^2}{H_3} \left(\frac{\psi_2 - \psi_3}{g'_2} \right) - \frac{f_0}{H_3} \eta_b \end{aligned}$$

These equations are commonly used for analysis of ocean flows, largely because of this relationship between the potential vorticity and the stream function, meaning one can be inverted numerically to find the other. This task has been undertaken several times for the stability analysis part of this project.

4 Data Assimilation

As outlined in [Karabasov et al., 2009], the PV anomaly data is defined over a square, flat-bottomed basin ($\eta_b = 0$), with rigid walls of length $L = 3840\text{km}$ bounding each side. The layers have thickness 0.25km, 0.75km and 3km respectively. The data is generated using a QG model similar to above; it is modified to include the forcing terms due to wind, viscosity in the third layer due to the fixed bottom topography (μ_{bot}) and eddy viscosity (μ_{eddy}). These are combined in the term:

$$F_n = \delta_{1n} f_{wind} - \beta v_n + \delta_{3n} \mu_{bot} \nabla^2 \psi_n + \mu_{eddy} \nabla^2 (\nabla^2 \psi_n)$$

where $\mu_{bot} = 4 \times 10^{-8} \text{s}^{-1}$, $\mu_{eddy} = 12 \text{m}^2 \text{s}^{-1}$, and the wind stress curl which drives the ocean circulation is given by

$$f_{wind} = \begin{cases} -1.80\pi\tau_0 \sin\left(\frac{\pi y}{y_0}\right), & \text{if } y \in [0, y_0) \\ 2.22\pi\tau_0 \sin\left(\frac{\pi(y-y_0)}{L-y_0}\right), & \text{if } y \in [y_0, L] \end{cases}$$

where $y_0 = 0.4L + 0.2x$ is the rising diagonal line from east to west.

Here $\tau_0 = 0.3 \text{N m}^{-2}$, and the density in the first layer is $\rho_1 = 1000 \text{kg m}^{-3}$ (or 1g cm^{-3}). Finally, the Coriolis parameter is $f_0 = 0.83 \times 10^{-4} \text{s}^{-1}$, and $\beta = 2 \times 10^{-11} \text{m}^{-1} \text{s}^{-1}$. (Note: The parameters used to generate this data and the wind forcing term were taken from [Shevchenko and Berloff, 2015].)

Then the potential vorticity anomaly is defined by the QG equations:

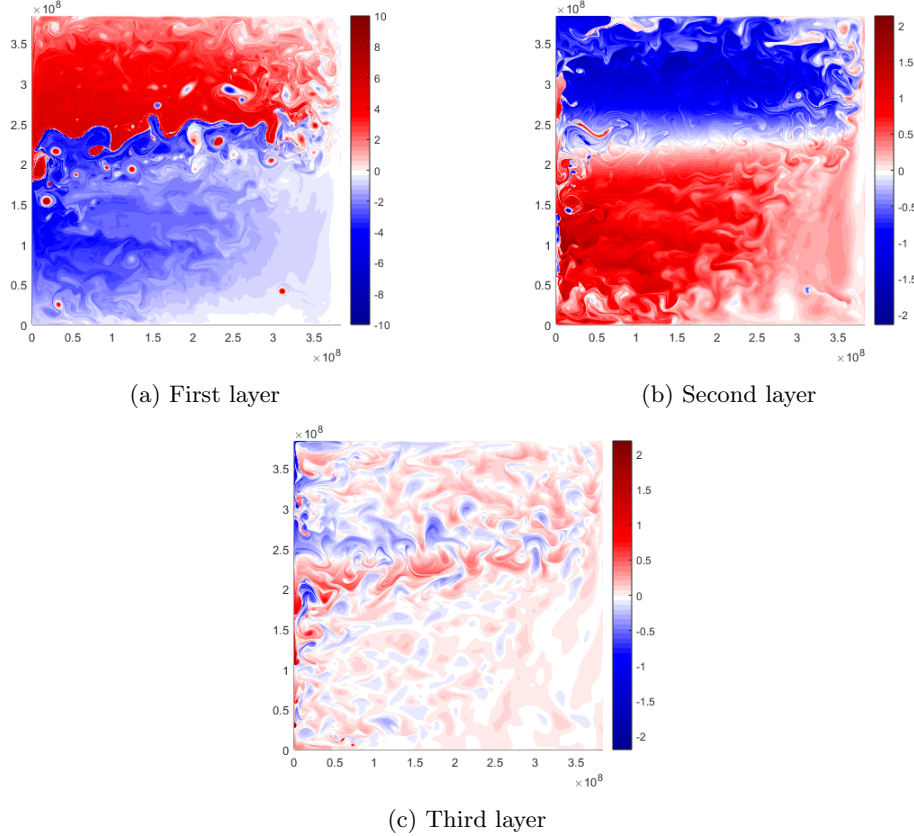
$$\begin{aligned} \frac{Dq_n}{Dt} &= F_n, \quad n = 1, 2, 3 \\ q_1 &= \nabla^2 \psi_1 + s_1(\psi_2 - \psi_1) \\ q_2 &= \nabla^2 \psi_2 + s_{21}(\psi_1 - \psi_2) - s_{22}(\psi_2 - \psi_3) \\ q_3 &= \nabla^2 \psi_3 + s_3(\psi_2 - \psi_3) \end{aligned}$$

Here the stratification parameters s_1, s_{21}, s_{22} and s_3 are chosen to specify the radii of deformation L_d .

The PV anomaly data that has been used in this project was generated by discretising these equations and taking snapshots of the evolution of the PV anomaly on each day. To set the initial condition, the value for the PV anomaly was set to zero and then the evolution algorithm was run for a long time period.

The data that has been used in this project is the three layers of QG potential vorticity anomaly over 422 days. There were some missing data files, so there were only 365 files altogether. In order to be able to analyse the motion of mesoscale vortices, the grid on which the CABARET model was used needed to be sufficiently fine. In fact, the grid divides the domain into 4097x4097 points, so that each cell is less than 1km in dimension.

Below we see the three layers of PV anomaly for the first day:



It is apparent from these images that the vortices are largely restricted to the first layer. Because of this, the data analysis for this project used only the first layer of PV anomaly, except where all three layers were required to calculate the stream function.

We note that in figure 1b there is a vortex in the southwest corner which is of opposite sign to the part of the vortex in the first layer. This is known as a Henton and is theorised to be of greater stability and hence potentially longer lifespan than other types of vortices. In this project, the three vortices which were found to be Henton which formed in the southwest corner were particularly long-lived. This is a topic for further research.

5 Obtaining and Sorting the Vortices

5.1 Vortex Extraction Algorithm

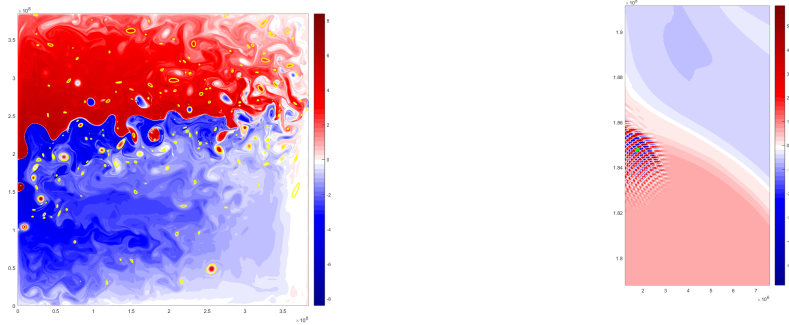
The vortices that have been used in this project were identified using the contour extraction algorithm developed by [Hadjighasem, 2015]. The algorithm takes as input a two-dimensional scalar field (which here is the top layer of the PV anomaly) and the grid on which this is defined (here the 4097 points from 0 to 3840km in the x and y directions), and three parameters which affect how many vortices are found. It then outputs a MATLAB cell structure containing the (x,y) coordinates of the vortex contours and the positions of their centres, as well as the value of the input scalar field at the centre.

5.2 Preparing the PV Anomaly Field

Initially, we attempted to use the vortex finding algorithm on the raw PV anomaly for each of the 365 available data files. However, this gave poor results for two main reasons:

1. The vortex extraction algorithm was unable to pick up many of the vortices as there was not enough contrast between the vortices' PV anomaly and that of the background flow.
2. The vortex extraction algorithm returned many anomalous results, returning 'vortices' which were in fact singular points of high PV anomaly in the flow.

Examples of both of these issues are given in the images below; the data used here was the day 5 PV anomaly, with 100 contour levels, a minimum arc length threshold of 1.15, and a deficiency thresh percentage of 100%.



(a) All vortices located

(b) A located vortex with the highest PV anomaly value at its centre

Figure 2: Anomalous results of the vortex finding algorithm when used on raw PV anomaly data

These two factors led to a two-step approach (Appendix section 9.1) to adjusting the PV anomaly field and optimising the number of vortices found and the accuracy of doing this. First, we subtracted the time-averaged flow from each data file for each day, in order to make the regions where PV anomaly was high compared to the background PV anomaly (i.e. the vortices) more apparent to the vortex extraction algorithm. After this, we smoothed out sharp spikes in PV anomaly, which were common in the first layer of the flow, by applying a moving average filter of degree 20.

An example of the process using the day 70 PV anomaly is illustrated below.

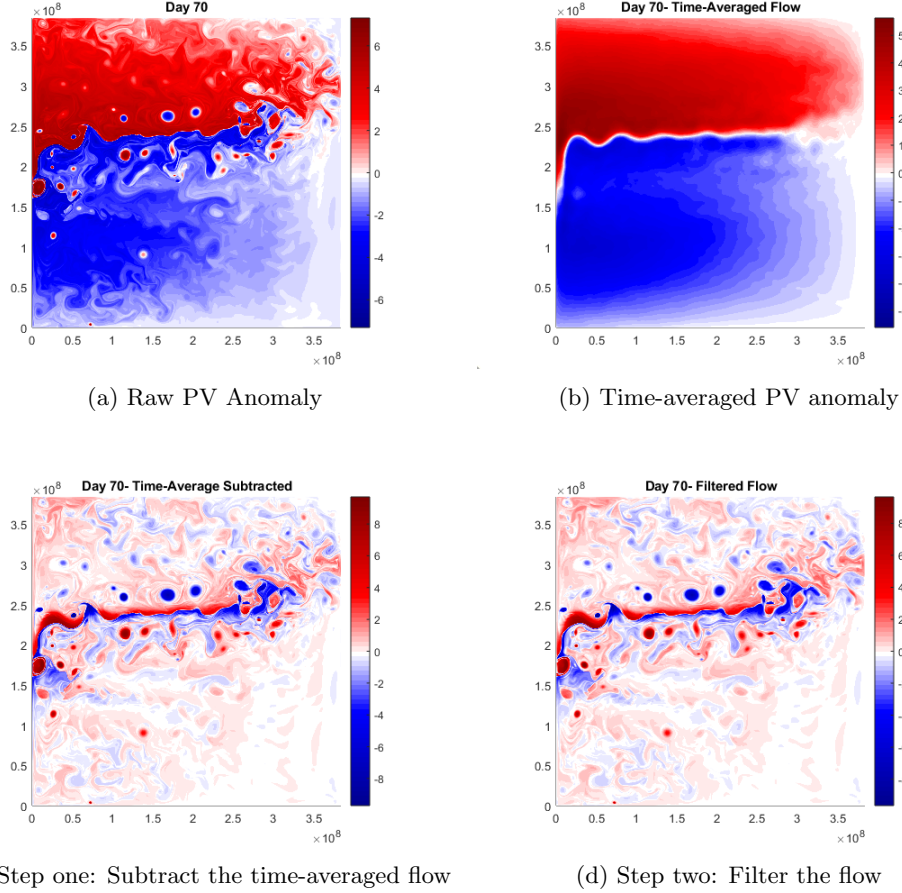


Figure 3: Data Adjustment Process

We can see from 3c that subtracting the average PV from each day makes the vortices considerably more apparent. This large contrast (and the absence of anomalous PV spikes due to filtering) led to a highly satisfactory performance of the vortex finding algorithm (see 6a).

5.3 Obtaining the Vortices

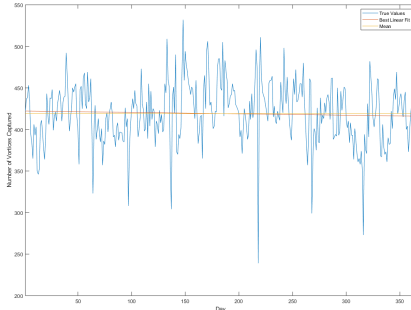
The process described in 5.2 was carried out for all data files. I then applied the vortex extraction algorithm to the 365 filtered PV anomaly flows (Appendix section 9.1).

Since the vortex finding algorithm works by finding the local maximums of the PV anomaly, the algorithm was used twice on each data file; first, to the unaltered data, and then to the inverted data (i.e. multiplied by -1). This resulted in two sets of vortices. They can roughly be described as the set of cyclones and the set of anticyclones. There was some overlap between the sets- however, as we will see in the next section, this turned out to be a very minor issue.

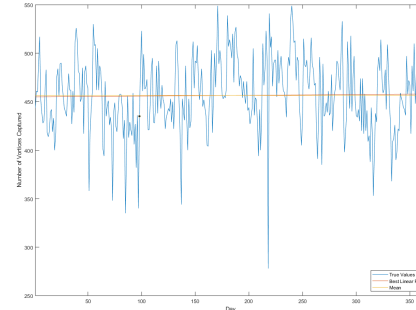
The vortices extracted by the algorithm are summarised in the table below.

Vortex Type	Total Number	Average Number Per Day	Linear Fit
Cyclones	152,961	419.1	$422.2 - 0.017x$
Anticyclones	166,609	456.5	$455 + 0.0079x$
All	319,570	438.6	

The distribution of the vortices found on each day was evenly distributed about the mean, with no noticeable difference in the variance for each vortex type:



(a) Cyclonic vortices found each day



(b) Anticyclonic vortices found each day

5.4 Sorting the Vortices

In order to remove the 'vortices' found by the algorithm which could not be regarded as such, and also to make the problem of tracking the vortices tractable, many of the 319570 vortices had to be discarded. Two thresholds were set for one of the 319,570 recorded vortices to be kept:

1. The vortex must have an area of over $14 \times 10^{12} \text{cm}^2$. For a circular vortex this corresponds to a radius of approximately 50 km or greater.
2. The PV anomaly at the centre of the vortex must be larger than 1.5.

Vortex Type	Total Number	Average Number Per Day	Linear Fit
Cyclones	7427	20.3	$21.5 - 0.0065x$
Anticyclones	9482	26.0	$24.5 + 0.008x$
All	16909	46.3	$46.1 + 0.0015x$

Table 1: Number of vortices in final set

This sorting algorithm (Appendix section 9.2) was applied to both sets of vortices, and the results are summarised in table 1.

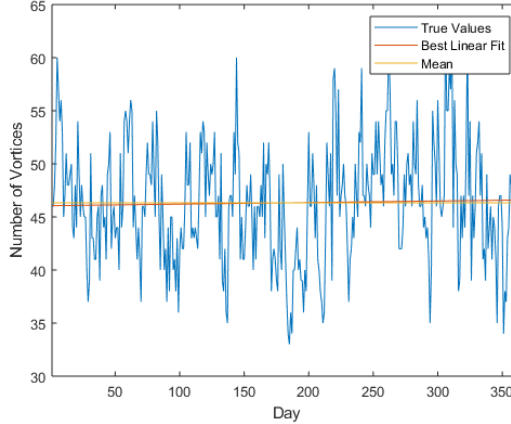


Figure 5: Variability in number of vortices per day in final set

The two sets of vortices were then combined into the final set. We can see in 5 that the resulting number of vortices for each data file actually deviates less from the mean than before, as we are no longer regarding the smaller fluctuations in the PV anomaly field as vortices (these were more susceptible to variability per day).

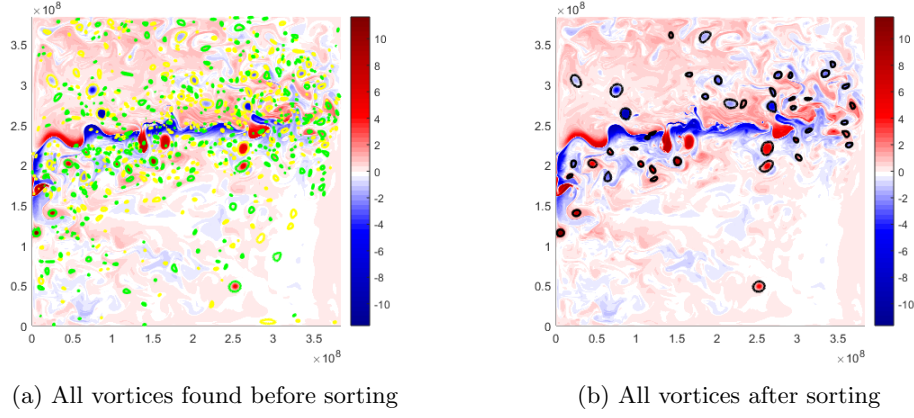


Figure 6: Vortices extracted from the adjusted PV anomaly field

In summary, the accuracy of the vortex tracker greatly increased after changing the scalar input field, as shown in figure 6a. However, it was still necessary to remove the smaller and weaker vortices so that only the major vortices were left (figure 6b). This meant that the problem of tracking the vortices was now solvable.

6 Tracking the Vortices

The problem next was to match up the coordinates of the vortex boundaries and their centres for each day into tracks of the paths the vortices travel over their lifespan.

The final tracking algorithm (Appendix section 9.3) takes as input the structure containing all information about the 365 days of vortices, and outputs a 3-dimensional matrix of tracks. Each row corresponds to the track of one vortex, containing the (x,y) coordinates of the centres, and each column represents one day.

The algorithm is as follows:

1. Initialise the tracks matrix as a matrix of zeros. Set the first column of the tracks matrix to be the (x,y) coordinates of the 46 vortices recorded for day 1.
2. Obtain the (x,y) coordinates of the track on the day that you are currently on. If no vortex was recorded (i.e. none could be found for this day), go to step 6.
3. For each vortex recorded for the day after this, calculate the Euclidean distance between its centre and the centre of today's vortex.
4. Sort the distances from smallest to largest and choose (up to) the three smallest which are below the threshold of 170km.
5. If no vortices are identified as close enough, move on to step 6. Otherwise:
 - a) Obtain the indices of the (three or less) nearby vortices in the record for the second day.
 - b) Obtain the PV anomaly values (for the filtered, time-average subtracted flow- see Notes) at the centre of these vortices
 - c) Calculate the difference between these values and the PV anomaly value at the centre of today's vortex
 - d) If the minimum difference in PV anomaly is below 0.75, set the coordinates of the vortex which has this smallest difference to be the vortex's position on the next day, and exclude this vortex from being tested again. Otherwise, go to step 6.
6. If no vortices were close enough or with a similar enough PV anomaly to the vortex of today, or no vortex was recorded for this track today, we use the vortex centre from the day before in its track (assuming we are not on the first day). As long as a vortex has been recorded:
 - a) Repeat the procedure in step 5, except use higher thresholds- distances of up to 240km and PV anomaly differences of up to 1.5.
 - b) If a suitable vortex is found from the next day, set its centre coordinates to be

the next point in the vortex's track, and exclude it from being tested again.

7. Repeat steps 2-6 for each vortex in this day's record.
8. Find all vortices from the next day which have not been matched up to a vortex from today. Place these coordinates in new rows at the bottom of the matrix for the next day, so that they may be used as the beginnings of their tracks.
9. Repeat the steps above for all days 1-364.

Notes on the Tracking Algorithm

- The thresholds for the distances were determined by observing video footage of the vortices and estimating the maximum distance travelled on each day.
- The PV anomaly thresholds were determined by trial and error, by applying the algorithm for a chosen threshold and then observing video footage of the tracks to see how the algorithm performed.
- The 'PV anomaly' values are actually not the true, raw values, but instead the vortex centre values recorded by the vortex finding algorithm when applied to the filtered, time-average subtracted flow. This is unimportant here, because we are looking at similarity of vortices and therefore it is only the magnitude of the values which is important.

The performance of this tracking algorithm was not perfect. However, out of the several that were developed, it was the best-performing by far.

Example of a Previous Tracking Algorithm

An outline of an older version of the tracking algorithm (which takes the same input and returns the same form of output) is given below:

1. Initialise the tracks matrix as a matrix of zeros. Set the first column of the tracks matrix to be the (x,y).
2. Obtain the (x,y) coordinates of the first vortex centre in the record of the vortices on the next day.
3. Calculate the Euclidean distance between this vortex and all of today's vortices.
4. Get the indices of all vortices that are less than 150km away:
 - a) If only one vortex is found, set the centre of the next day's vortex as the next

position in its track.

- b) If more than one vortex is found, calculate the difference in PV anomaly (for the filtered, time-average subtracted flow) and if the vortex with the minimum difference in PV anomaly is below 0.5, set the centre of the next day's vortex as the next position in its track.
 - c) If no vortices are found to be similar enough, repeat the procedure using all of yesterday's vortex positions- assuming that it has been recorded. The thresholds for distance and PV anomaly difference are 200km and 0.8 respectively.
 - d) If the next day's vortex cannot be matched up, place it in a new row at the bottom of the matrix to represent the formation of a vortex.
5. Repeat for all vortices in the next day's record.
 6. Repeat for all days 1-365.

Refining the Tracking Algorithm

There were several problems with this algorithm and the previous attempts, which the final algorithm was largely able to resolve.

Firstly, there was an issue due to it being a "backwards-looking" algorithm, i.e. the fact that it focused on the next day's vortex and tried to match it up with the positions already stored in the tracks. This meant that the vortices were not being excluded as they were matched up, and so there was often overwriting of the tracks with another nearby vortex. In the end, it would be the last vortices of the next day which were stored in the matrix, and many of them would have been deleted.

This issue was further exacerbated by the immediate allocation of a vortex to a track if it was found to be the only vortex close enough. This meant that if the true vortex in the track happened not to be picked up by the vortex finding algorithm on this day, it would likely be replaced by an incorrect vortex and hence the real track would be lost.

These problems resulted in a tracking algorithm which would return what looked at first glance to be good results, that is, a small number of tracks which would suggest the vortices were being well matched up.

However, the reality was that the tracking algorithm was not discerning enough and was linking together vortices that were not actually the same. This behaviour could easily be observed by creating video footage of the tracks. This explains the relatively low thresholds used for distance and PV anomaly difference in the algorithm- it was initially thought that these limits were too lenient and this was causing the lack of precision.

The final tracking algorithm was designed with the aim of rectifying these problems. Firstly, it uses a forward-looking approach- choosing the vortex from the present day and

scanning the vortices of the next day to see if a match can be found. Since the next day's vortices are not already in the matrix of tracks, they can be removed as they are matched up, preventing the problem of overwriting.

Secondly, the final algorithm uses two conditions to ascertain that two nearby vortices were truly the same- both distance and PV anomaly distance, even when only one potential vortex is found. This greatly decreases the likelihood that a track will switch to a different vortex.

Comparison of the Two Algorithms

Table 2 shows that, as stated, the backwards algorithm appears to pick up longer and fewer tracks. This is because of the leniency of the algorithm in assigning a vortex to a given track. On the other hand, the forwards algorithm matched up fewer algorithms but the tracks it produced were considerably more accurate. For this reason it was the algorithm used to generate tracks from which the vortex properties were derived.

Algorithm Type	Number of Tracks	Average Length of Track (Days)
Backwards	2429	6.97
Forwards	4504	4.63

Table 2: Comparison of tracks produced by the two algorithms

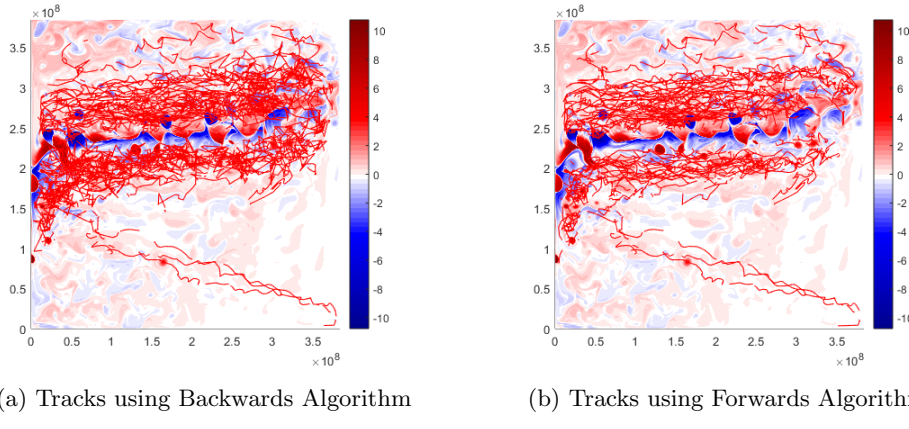


Figure 7: Comparison of the tracks generated by the algorithms which were twenty days or longer. The tracks are denser for the backwards algorithm in the region surrounding the jet, where the vortices are concentrated and regularly interact and pass close to each other. The less discerning approach of the backwards algorithm meant that the tracks it produced often jumped from vortex to vortex.

7 Results

7.1 Characteristics of the Population

We now discuss the observed properties of the entire population of vortices, namely the tracks, lifespans, formation and termination points, average speeds and areas, and the energies and energy densities (calculated using code in Appendix 9.4).

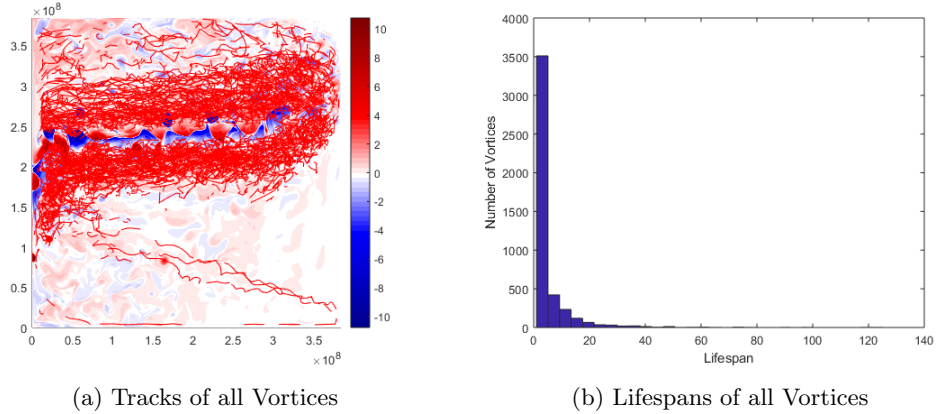


Figure 8

The tracks of the vortices, as shown in 8a, were found to be densest at a distance of hundred kilometres from the jet, and they did not tend to venture more than 600km away to the north and south. The general trend was for the vortices to propagate eastwards, i.e. in the opposite direction to the jet. Due to the density of vortices in this region, there were few which did not interact with other vortices during their lifespan, and there were often cases of vortices merging and (less frequently) splitting.

We can see that there were only three vortices which followed a different path. These were all cyclonic vortices which emerged at the eastern side of the jet and travelled at speed along the southern and western rigid walls, and then travelled northeast until finally being absorbed back into the jet. Although these were clearly unrealistic and arose only due to the rigid boundaries, they did provide an opportunity to assess the behaviour of isolated vortices.

The distribution of the lifespans of the vortices are illustrated in 8b and were defined as the true number of days (calculated using the function in section 9.6) between the tracking algorithm picking up and then losing a vortex. 49.8% of vortices were tracked for just one day, and a further 23.9% were tracked for between 2 and 4 days. It was often the case that the vortices emerged from the jet to be quickly reabsorbed, however undeniably this reflects the imperfection of the tracking algorithm. Still, in some cases the algorithm was highly successful, resulting in a maximum observed lifespan of 125 days.

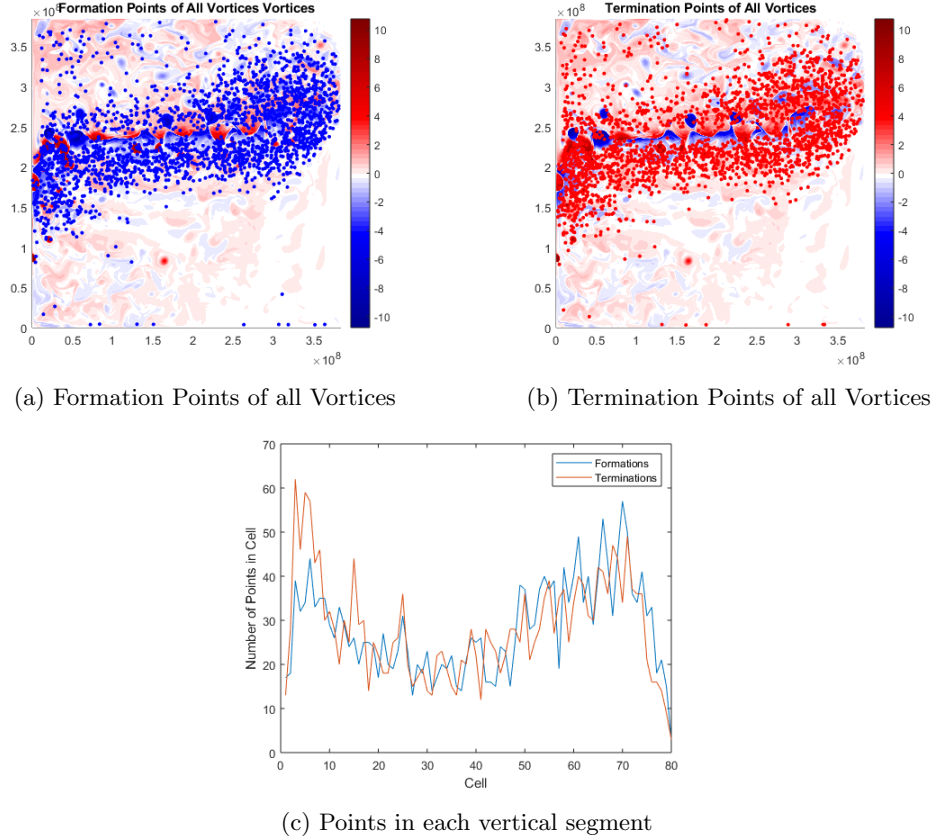


Figure 9: The formation and termination points are defined as the first and last points respectively in each track provided by the algorithm. These are shown in 9a and 9b against a snapshot of the filtered flow for all vortices tracked for two days or longer (to ensure no identical points are plotted). As expected, they are densely clustered around the jet. Figure 9c shows the number of points per section when the domain is split into 80 vertical rectangles. We can see that there are more vortices forming in the west and terminating in the east, which reinforces the observations of vortices travelling in this direction. The slight 'out of phase' pattern in the eastern sections may result from vortices being picked up for just two or three days in which time they have moved slightly westwards. Both formations and terminations are greater at near the horizontal boundaries than at the middle of the jet, suggesting these boundaries play a part in introducing and dispersing vorticity in the flow.

Now we look at the average areas, speeds and total distances travelled. The methods used for calculating these quantities was as follows:

- The area was calculated as the average of the areas inside the contour given by the vortex finding algorithm at each step in the track.
- To obtain the speeds, first any missing points in the vortex's journey (due to the missing PV anomaly files or gaps in the track) were estimated by linear interpolation. Then the Euclidean distance was calculated between points in the track to get an average speed per day, and then the average of all these speeds was taken. Plots of speeds for individual vortices showed a high level of noise, even for the isolated vortices.
- The total distance travelled was found by summing the distances travelled per day. If the vortex was tracked for one day, the total distance was registered as zero.

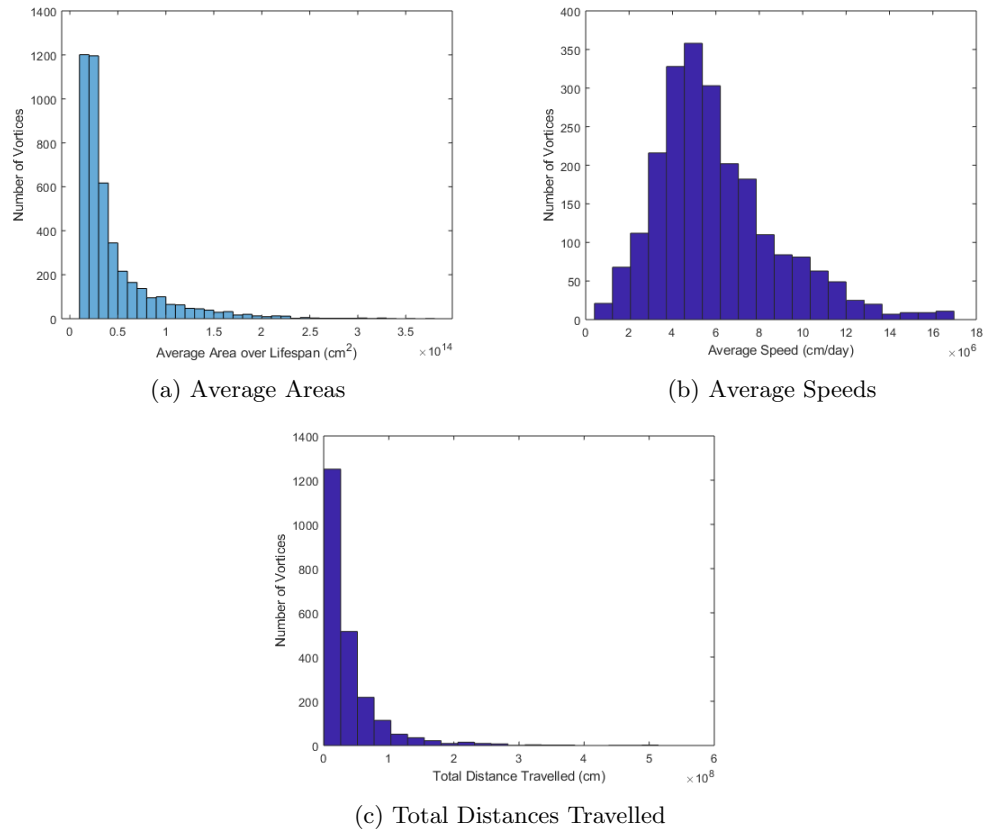


Figure 10

The distribution of the areas and distances travelled take a similar distribution to the lifespans, potentially suggesting a connection- (see next section). The mean area of the vortices was $4.5 \times 10^{13} \text{ cm}^2$, which is can also be interpreted as a radius of $3.78 \times 10^6 \text{ cm}$ if we take the vortices to be quasi-circular. It is likely many of the smaller areas corresponded to the weaker vortices which were not picked up by the tracking algorithm for long, because their evolutions and predecessors were discarded as too small in the sorting process.

The total distance for all vortices was $1.93 \times 10^7 \text{ cm}$, i.e. just over twice the average diameter of the vortex. However, this is distorted by the presence of day-long vortices with zero distance. Ignoring these, the average is $3.84 \times 10^7 \text{ cm}$, which corresponds to five times the average diameter of the vortices with non-instantaneous tracks.

Finally, the average speeds were more evenly distributed either side of their mean of $6 \times 10^6 \text{ cm/day}$, with a tail on the right suggesting there were several outlying cases of particularly fast-moving vortices. Note that speeds were only defined for vortices which were tracked for longer than one day.

7.1.1 Energies and Energy Densities

The energy of each vortex at an instant was calculated using an approximation of the formula for kinetic energy:

$$KE = \frac{1}{2} \int_{\Omega} \underline{u}^2 dx$$

Here the domain Ω is the 3840km x 3840km square top layer. To calculate the eddy kinetic energy as stated in [Shevchenko and Berloff, 2015], we take the difference of the velocity with the time-averaged velocity and sum the squared components of this over all points in the 4097x4097 grid which fall within the contour selected by the vortex finding algorithm. Then we can calculate the average energy as the mean of the energies of the vortex at each time-step in its track. The results are dimensionless quantities, i.e. they have no units.

We also calculated the energy densities of the vortex at each instance, as well as its average. To do this, we simply normalised the energy at each time-step by the previously calculated area of the vortex, and averaged over this. The energy density was found to be considerably less noisy than the energy, and to better describe the events of the vortex's life (such as interactions, the combining of two vortices as well as steady decay) and we will use it in more detail when analysing the long-lived vortices in section BLAH.

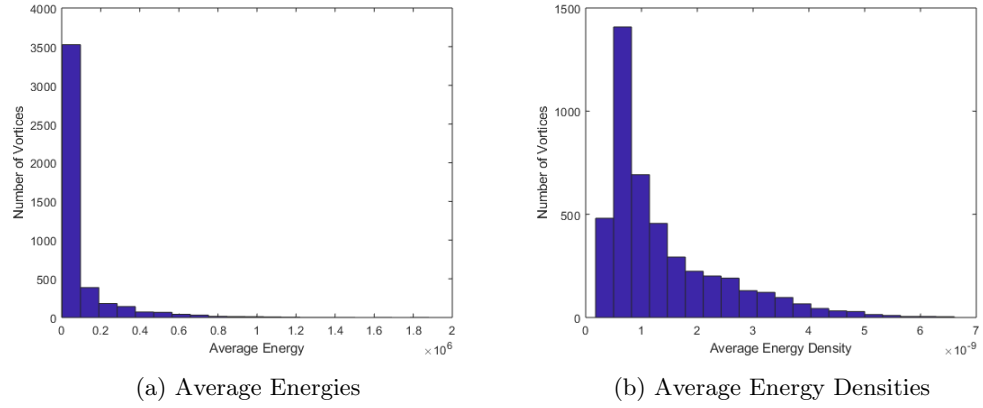


Figure 11: The average energies shows a similar distribution to the lifespans, areas and total distances travelled. The mean of all average energies is 9.15×10^4 , yet the median is just 2.8×10^4 illustrating the skewed nature of the distributions. The vortex of maximum has an energy over twenty times larger than the mean at 1.88×10^6 , (This extremely high energy vortex is one of the largest in the population and is tracked for just one day.) Since the energy is dependent on the area of the vortex, we turn to the energy densities to compare vortices of different sizes. This has a more even distribution around its mean of 1.4×10^{-9} , although we can see from the histogram 11b that the median is much less than this; in fact only 35% of the vortices have an energy density greater than the mean. Thus the population is made up mainly of similarly low energy density vortices with a small number of outlying highly energetic cases.

7.2 Effects of Characteristics on Vortex Lifespan

In this section, we move on to observing the relationships between the aforementioned variables, in the hopes of determining trends or correlations.

Other	Lifespan	Area	Speed	Distance	Energy	E Density
Lifespan	1.0000	0.3382	-0.0836	0.9554	0.1774	0.1065
Area	0.3382	1.0000	-0.0971	0.3160	0.8682	0.6360
Speed	-0.0836	-0.0971	1.0000	0.1546	-0.0303	0.0101
Distance	0.9554	0.3160	0.1546	1.0000	0.1783	0.1181
Energy	0.1774	0.8682	-0.0303	0.1783	1.0000	0.8703
E Density	0.1065	0.6360	0.0101	0.1181	0.8703	1.0000

Table 3: Pearson correlation coefficient for all pairwise combinations of the averaged characteristics of vortices which are tracked for longer than five days.

Table 3 shows the strength of the linear correlations between all variables. We use only tracks which are over 5 days long, in order to have more reliable averages. We see that there is an almost perfect linear correlation between the lifespan and the total distance travelled by a vortex (see figure 14b). This is of course to be expected since the distance is calculated by summing the distance travelled each day. In a similar way there is the strong correlation between area and energy, since a larger area means a larger area to sum the (non-negative) squared velocity components over.

Furthermore, there appears to be a minor correlation between the lifespans and the average areas, which should also be investigated. Aside from this, the correlations between lifespans and the other variables are weak to negligible.

We note that the energy density is still correlated with the average vortex area despite the fact that the area is used here to normalise the energy. It is also apparent that the speed is linearly related to no other variable, except perhaps a minor relationship with the distance travelled, since a vortex which is moving faster each day will return a greater value of these summed distances.

Over the next few pages, we will investigate these correlations and whether other non-linear patterns arise between the variables.

Figures 12 and 13 on the next page show the tracks, formations and terminations of the long-lived vortices. It appears that the longest-lived (or at least the longest-tracked) vortices are those that originate at the east of the jet and pass at a distance above (or occasionally a distance below) the jet before terminating in the west.

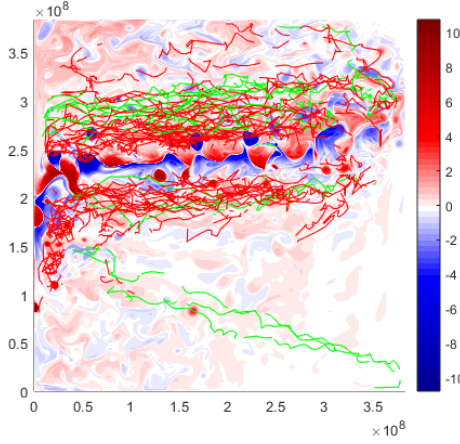


Figure 12: Tracks of the long-lived vortices- red represents those between twenty and fifty days long, and green is for vortices which are tracked for more than fifty days. Almost all the tracks travel parallel to the jet at a distance of between 200-600km. In particular, the more distant southern tracks do not feature. The most noticeable trend is that the green, longest-lived vortices all pass at a considerable distance from the jet. This is likely to be due to the fact that that they avoid interacting with, and hence being absorbed by, the jet, which is a danger for the vortices which pass close to it. Finally, the three isolated vortices, who have no other major sources of vorticity to interact with, all live longer than fifty days.

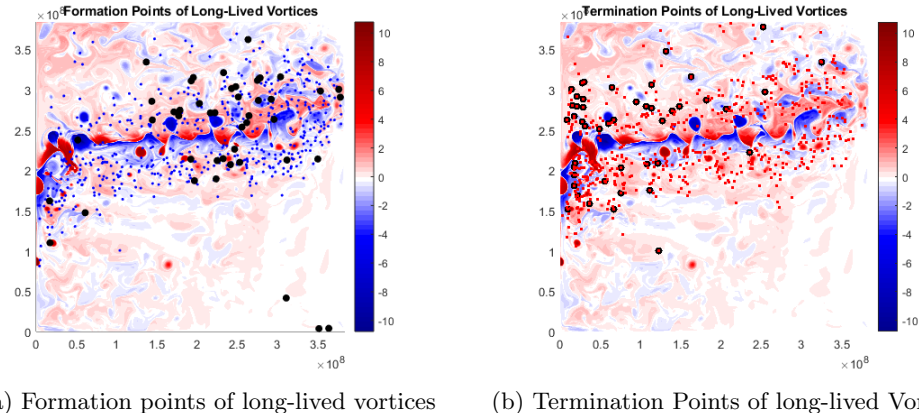
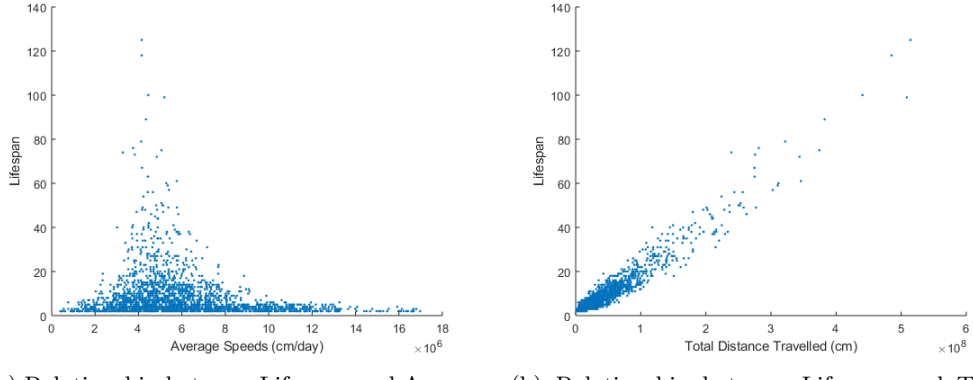


Figure 13: Depicted are the formations and terminations for vortices living for over ten days. The black larger points represent vortices living for over forty days. We see that the trend of vortices forming at the east and terminating at the west is more pronounced for these long-lived vortices.



(a) Relationship between Lifespan and Average Speed (b) Relationship between Lifespan and Total Distance Travelled

Figure 14

Although no linear relationship was established between the speeds and lifespans of the vortices, figure 14a shows that there is indeed a non-linear relationship. The longest-lived vortices seem to have average speeds that are very close to each other, despite the differing environments that their tracks take place in. For example, the two longest-lived vortices are isolated from other regions of concentrated PV anomaly, yet their speeds are similar to vortices which travel just north of the jet.

The long tail on the right hand side of the scatter plot suggest that the fastest-moving vortices were not tracked for a long period of time. This could be because they were moving faster than the distance threshold on the tracking algorithm, although this was up to 170km which, from video observation, was above the upper limit of the vortex speed. It is more likely that these large jumps represent the tracking algorithm switching between vortices, perhaps because the true next vortex in its track was not found by the vortex extraction algorithm. Finally, it could be that these fast-moving vortices were those that were travelling close to the jet (and therefore being propelled quickly forward) and hence were quickly reabsorbed.

As was seen in table 3, there is a strongly positive linear correlation between the lifespans and the distances travelled. The fact that the longest-lived vortices all have similar speeds contributes to this fact. The clustering of points in the bottom left corner represents the fact that a large proportion of the vortices were tracked for only a day or two and therefore their calculated distance was close to zero.

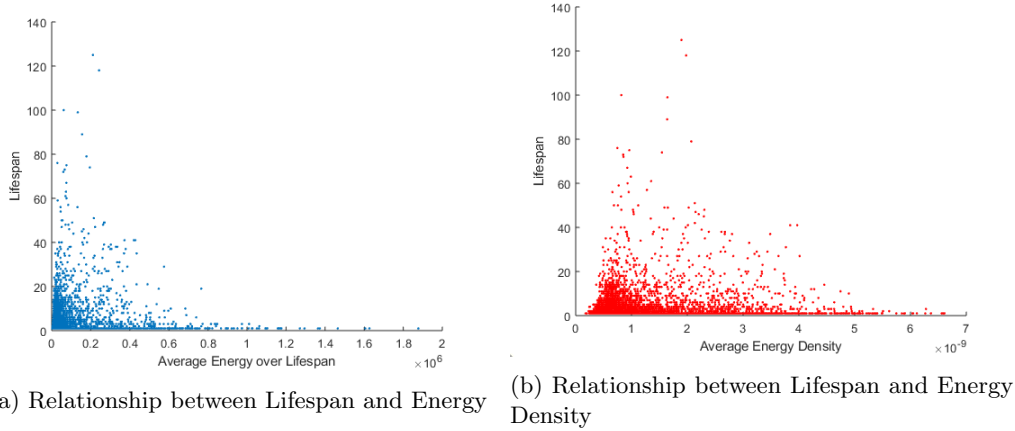


Figure 15: There does not appear to be a strong relationship between the energies and energy densities and the lifespan of the vortex. On the other hand, the long-lived vortices all have energies that are towards the low end of the range. As the lifespan decreases the range of possible average energies increase. The highest energy vortices are all short-lived. The energy densities are more variable for the population, suggesting this normalized energy is a better method for comparing vortices.

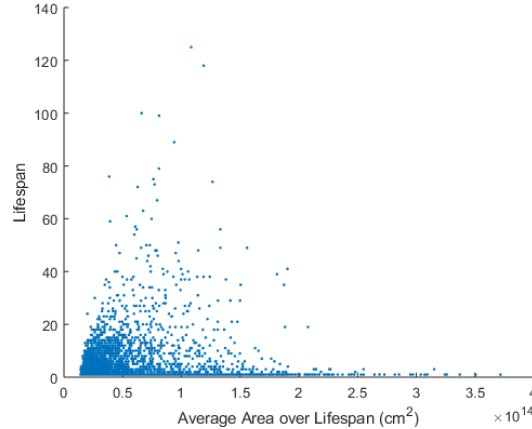


Figure 16: Relationship between Lifespan and Area

The longest-lived vortices have areas roughly between $0.5 \times 10^{14} \text{cm}^2$ $1.5 \times 10^{14} \text{cm}^2$. The majority of vortices have areas less than $0.5 \times 10^{14} \text{cm}^2$ and these are generally short-lived. It is likely these were only briefly picked up by the tracking algorithm because their past and future vortices were too small to be included in the analysis, and yet they formed the bulk of the population.

7.3 Comparison of Cyclonic and Anticyclonic Vortices

We split the vortices into cyclones (having positive vorticity) and anticyclones (having negative vorticity) using the values provided for each vortex by the vortex finding algorithm (see Appendix 9.5). There were slightly more anticyclones than cyclones (2356 vs 2148).

We now investigate the contrasts and similarities between the characteristics of cyclonic anticyclonic vortices. Firstly, we compare the tracks, formations and terminations.

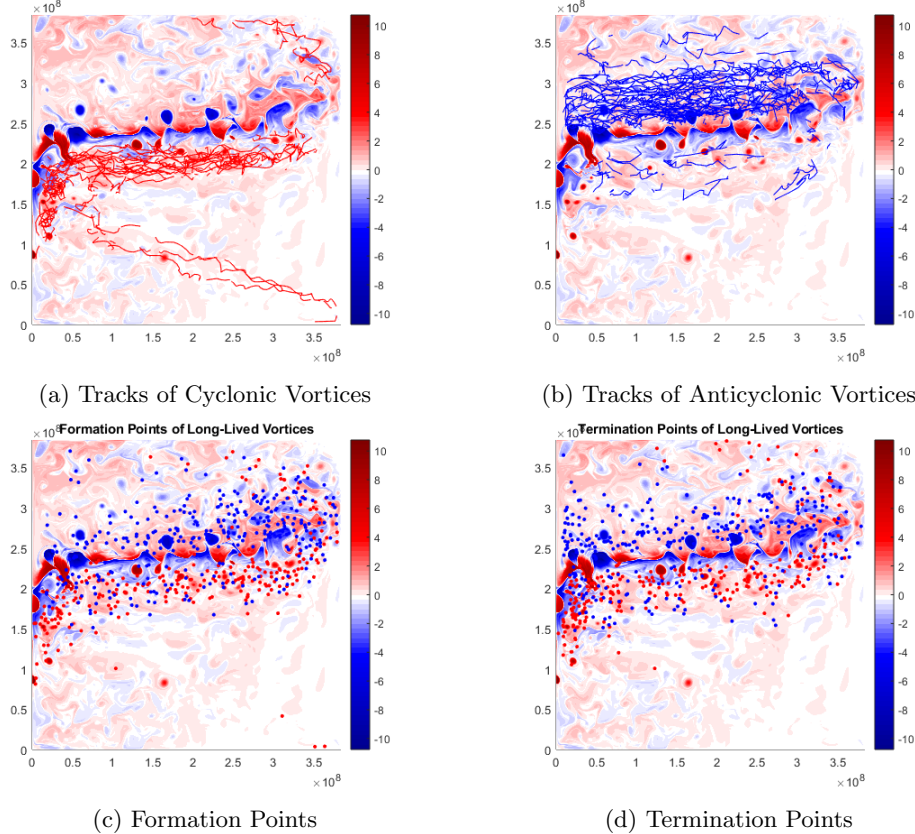
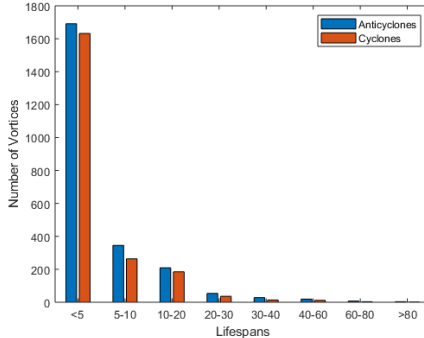
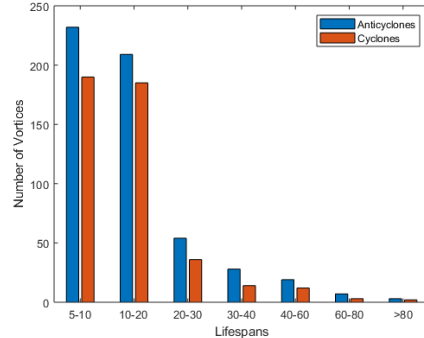


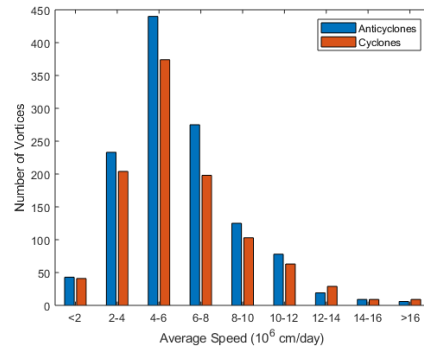
Figure 17: It is immediately obvious that in general, the cyclones pass below the jet, while the anticyclones pass above, as was suggested in [Carton, 2001]. The three isolated vortices are therefore cyclonic as expected. The anticyclones appear to be more far-reaching in the paths they take, passing eastwards further from the jet. It follows from the separation of vortex types that the cyclonic vortices form and terminate below the jet while the opposite is true for the anticyclones. Finally, it appears that there are more anticyclonic vortices spilling onto the southern side of the jet- this is a much rarer occurrence for cyclones.



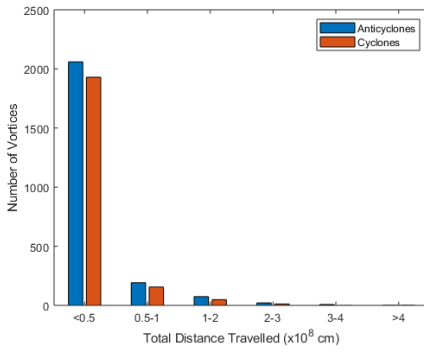
(a) Comparison of Lifespans



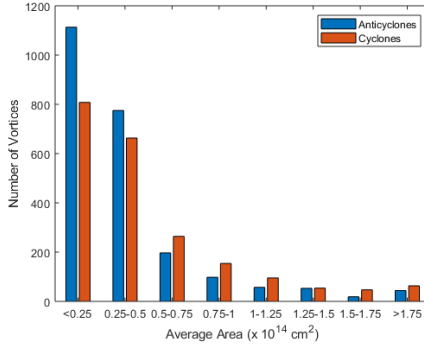
(b) Lifespans greater than 5 days



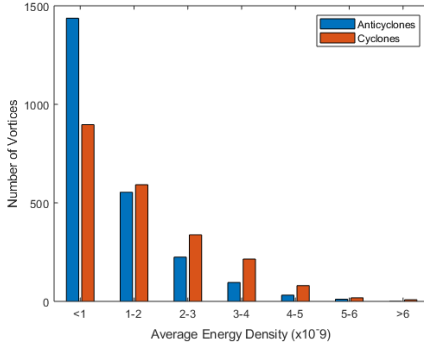
(c) Comparison of Average Speeds



(d) Comparison of Distances Travelled



(e) Comparison of Areas



(f) Comparison of Energy Densities

Figure 18: The shapes of the distributions for all characteristics shows little difference between cyclones and anticyclones. The cyclones lived for less time, with a mean of 4.26 days and a standard deviation of 7.6, compared to 4.96 days and a standard deviation of 8.5 for anticyclones. This may be because the anticyclones were more likely to travel further from the jet. As the strong correlation would imply, this led to anticyclones being tracked for a greater distance. The anticyclones were smaller on average ($4.0 \times 10^{13} \text{ cm}^2$ compared to $5.0 \times 10^{13} \text{ cm}^2$). In terms of average speed, the mean was almost identical at $6 \times 10^6 \text{ cm/day}$, but the spread for the cyclones was greater.

7.3.1 Relationship Between Characteristics

As we did for the entire population, we now briefly examine how the variables affect each other and if there are any contrasts between cyclones and anticyclones.

Other	Lifespan	Area	Speed	Distance	Energy	E Density
Lifespan	1.0000	0.3294	-0.1643	0.9661	0.1935	0.1268
Area	0.3294	1.0000	-0.1068	0.3082	0.8686	0.5973
Speed	-0.1643	-0.1068	1.0000	-0.0058	-0.0381	0.0117
Distance	0.9661	0.3082	-0.0058	1.0000	0.1940	0.1358
Energy	0.1935	0.8686	-0.0381	0.1940	1.0000	0.8286
E Density	0.1268	0.5973	0.0117	0.1358	0.8286	1.0000

Table 4: Pearson correlation coefficients for all pairwise combinations of averaged characteristics for all anticyclones in the population.

Other	Lifespan	Area	Speed	Distance	Energy	E Density
Lifespan	1.0000	0.1887	-0.1892	0.9599	0.0744	0.0544
Area	0.1887	1.0000	-0.0920	0.1732	0.8890	0.6318
Speed	-0.1892	-0.0920	1.0000	-0.0202	-0.0356	0.0402
Distance	0.9599	0.1732	-0.0202	1.0000	0.0684	0.0678
Energy	0.0744	0.8890	-0.0356	0.0684	1.0000	0.8333
E Density	0.0544	0.6318	0.0402	0.0678	0.8333	1.0000

Table 5: Pearson correlation coefficients for all pairwise combinations of averaged characteristics for all cyclones in the population.

We can see from the above tables that the correlations are largely similar for both vortex types. The main difference is that the lifespan and area are more closely connected for anticyclones, which inevitably leads to distances and areas being more correlated. Lastly, it appears that the energy has a slight correlation with the lifespan for anticyclones, while this is not the case for cyclones.

In summary, it would appear that connections between some of the variables are slightly stronger for anticyclones. This could be because they tended to live longer/be tracked for longer and so their averaged characteristics are more accurate.

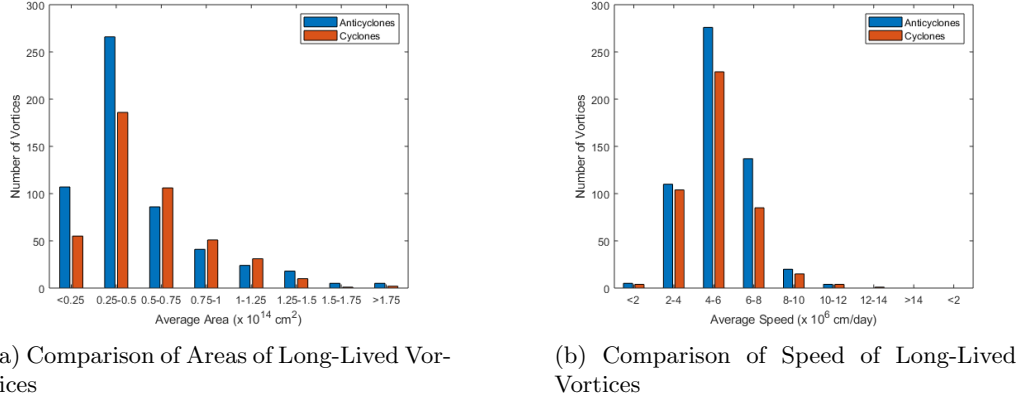


Figure 19: Areas and Speeds for Vortices Living Longer than 5 days

We examine the distributions of the areas and the speeds for the two vortex types with lifespans greater than 5 days to determine if there are differences to when short-lived vortices were included. It is apparent that for the entire population (regardless of sign), the mean has shifted upwards. This is partly due to the fact that small vortices were removed and so vortices which were on the size borderline may have had some time-steps in their lifespan removed from the population and thus appear short-lived. It may also be that larger vortices are more likely to absorb other vortices instead of being absorbed themselves, or be more able to resist being dispersed in the jet. The distribution of the anticyclone population's areas is more focused at the mean, whereas the cyclones' area distribution is more skewed, containing a greater proportion of large vortices.

The impact of removing the short-lived vortices on the distribution of the average speed is that, although the mean is unchanged, the tails have all but disappeared. The fact that the outlying speeds must belong to the short-lived vortices is a suggestion that they are caused by the tracking algorithm jumping large distances from one vortex to another, and therefore these high speeds could be a sign of an anomalous track. Finally, we can see there is a tendency for longer-lived anticyclones to tend towards higher speeds, and the opposite is true for cyclones.

7.4 Analysis of Long-Lived Vortices

In this section, we examine the particular characteristics of the ten longest-lived vortices, and examine how their energy densities are related to the events that take place during their lifespan.

Number	Lifespan	Position	Area	Speed	Energy Density	Interactions
1	125	Far below jet	1.08	4.15	1.89	None
2	118	Far below jet	1.19	4.15	1.98	None
3	100	Above jet	0.66	4.45	0.82	Several
4	99	Above jet	0.81	5.19	1.64	Several
5	89	Above jet	0.94	4.34	1.63	Several
6	79	Above jet	0.81	4.13	2.07	Several
7	76	Below jet	0.39	3.75	0.75	Several
8	75	Above jet	0.76	5.06	0.96	Several
9	74	Far below jet	1.27	3.28	1.54	None
10	73	Above jet	0.77	3.82	0.83	Several

Table 6: Characteristics of the Ten Longest-Lived Vortices

Observations of video footage of the vortices showed that vortex 7 was a highly anomalous track, and so it was not included in this analysis.

Due to similarities in average energy densities, areas (see table 6 and tracks (see figure 20), we decided to group the long-lived vortices as follows: Group 1 contained the isolated vortices 1,2, and 9; Group 2 contained the low energy vortices 3, 8 and 10; and Group 3 contained the mid energy vortices 4,5 and 6.

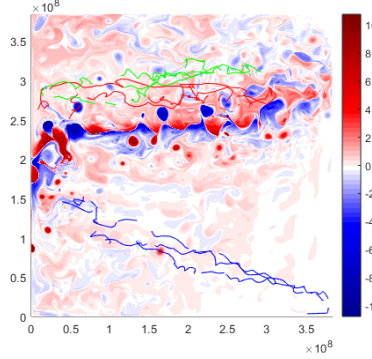


Figure 20: Tracks of the Ten Longest-Lived Vortices. Group 1 = Blue, Group 2 = Green, Group 3 = Red.

Group 1 Vortices

These three cyclonic vortices moved from the southwestern corner to the western end of the jet, one after the other. They were far removed from any other concentrated regions of vorticity until the end of their lifespan. In 21b we can see that the energy density of each vortex exponentially decays in a similar pattern with little noise until the vortex reaches the jet. This reflects that there are no other vortices to interact with in order to gain or lose energy.

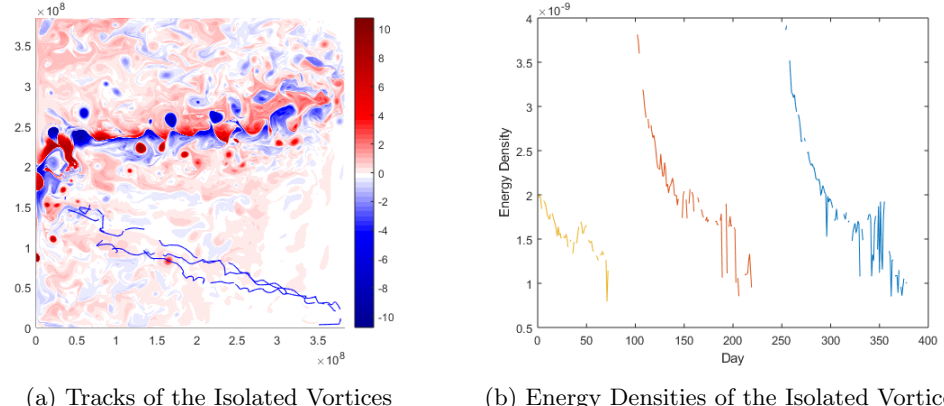


Figure 21

Group 2 Vortices

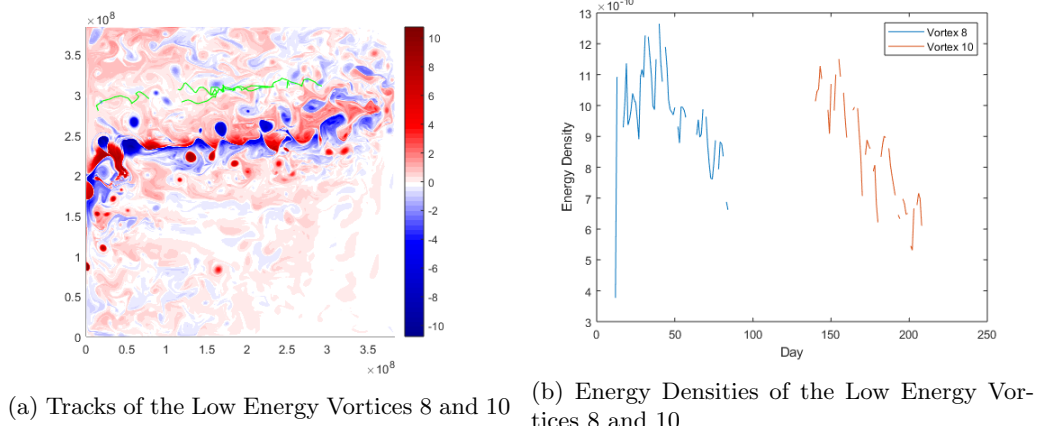
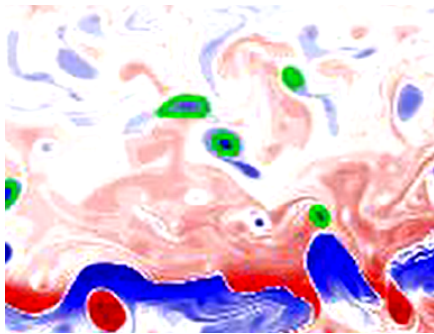


Figure 22

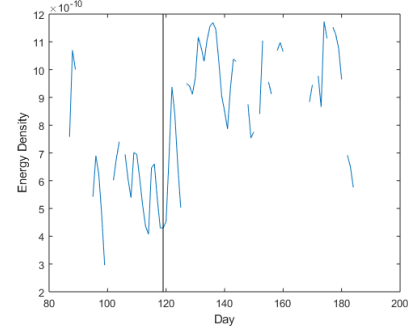
For this group, we looked at the vortices 8 and 10 together and then vortex 3 separately. The vortices were all anticyclones and took paths around 500km above the jet. The vortices 8 and 10 occasionally passed other vortices but never strongly interacted with them. We see this reflected in their energy density patterns in figure 22b, which are noisier than for the isolated vortices but have no great changes, instead displaying a steady downward trend.

In contrast, vortex 3 combined with two other vortices in a process that took several days from around 118-120, which is marked by a straight line on figure 23b. We notice that there was an initial decrease in energy as the merging took place and then a strong gain which was maintained for the rest of the vortex's life. After this point the vortex had increased greatly in size.

It is interesting to note that vortex 3 dies by colliding with the jet, whereas the other vortices faded away of their own accord. This could explain the sharp decrease in the energy density at the end of vortex 3's life.



(a) Vortex 3 combining with two other vortices on day 119



(b) Energy Density of Vortex 3

Figure 23

Group 3 Vortices

Finally, we investigate the energy densities of the vortices in the third group. These anticyclonic vortices were of higher energy density and passed closer to the jet than the vortices in group 2.

Vortices 4 and 5 were more similar in terms of average energy density and their energy density patterns, as is clear in 24b. The black line intersecting vortex 4's energy density represents the point at which the vortex combined with another of equal size, initially losing energy and then returning to its original level- further evidence that interactions impact a vortex's energy density. In slight contrast, the black lines for vortex 5 represent points where the vortex seemed to become partially joined with another vortex for a short period and then pulled away. We can see that this also appears to affect the energy density of the vortex. In this case it could be that the tracking algorithm briefly moves onto the other vortex, making it appear that the vortex's energy density has changed.

The tracking of vortex 6 starts by being quite anomalous, explaining the range of energy density values it takes. After the vortex properly emerges from the jet, it splits up and loses some of its PV, and this period is marked by the black line. We see that the loss of PV anomaly and subsequent decrease in size results in an increase in energy density.

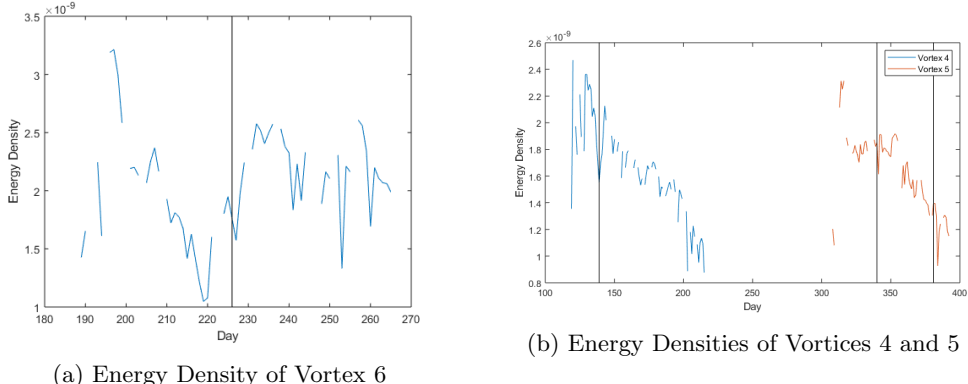


Figure 24

Summary

To summarise, we have been able to use the long-lived vortices to form a connection between energy density and interactions. It appears that the processes of merging and splitting can cause a vortex to increase its energy density, and that even short-term interactions have their effect. We have also seen that an isolated vortex will have a steadily decreasing energy density with no jumps or major fluctuations.

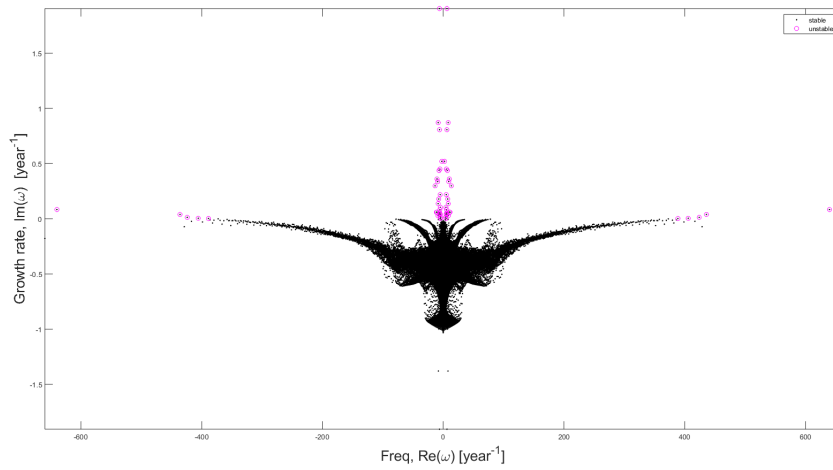
7.5 Stability Analysis

Several of the vortices were analysed using the linear stability solver described in [Shevchenko and Berloff, 2017] on the stream function found by inverting the PV anomaly isolated around the vortex (and zero everywhere else and in the two bottom layers). These vortices were as follows: one of the long-lived, isolated vortices in Group 1 (section 7.4); a snapshot of a vortex in the process of interacting with the jet; and two vortices before and after merging into one. The spectrum of the 271803 eigenvalues shows clear contrasts, especially between the isolated vortex and the other types. This shows that it may be possible to characterize the situation a vortex is in by its eigenvalue spectrum.

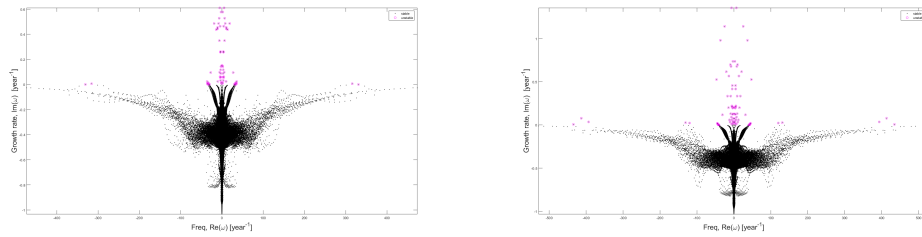
Figure 25 shows the eigenvalue spectra of the isolated vortex (for which there were 54 unstable eigenmodes), the two vortices as they merge (for which there were 68 and 84 unstable eigenmodes) and the combined vortex just after the merging has taken place (for which there were 80 unstable eigenmodes).

We note that all the spectra have roughly the same shape. The isolated vortex has the least number of unstable modes and was also a steady, long-lived vortex. Its spectra has a compact appearance. In contrast, the other three vortices have more unstable modes and their modes are more spread out, giving a shaky appearance. This is less apparent in the merged vortex. It could be that the merging vortex is returning to a state of stability similar to the first vortex.

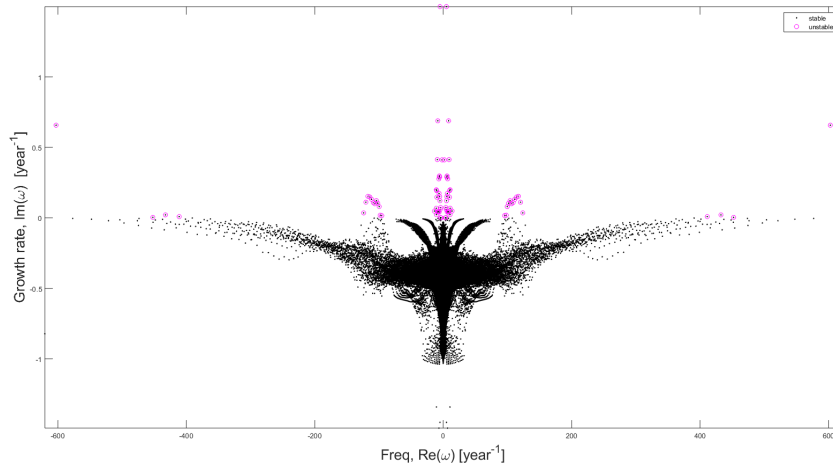
Overall, the eigenvalue spectra gives weight to the idea that the stability of a vortex is related to its lifespan, since the appearance of the steadily-moving vortex is quite different to the spectra of the others which are in transition periods. However, it could also mean that the vortex undergoes instability processes during merging and then returns to a more stable spectra. This is something that should be further investigated.



(a) Eigenvalue Spectrum of Isolated Vortex



(b) Eigenvalue Spectrum of Merging Vortex 1 (c) Eigenvalue Spectrum of Merging Vortex 2



(d) Eigenvalue Spectrum of Merged Vortex

Figure 25

8 Conclusion

In this project, we have studied how the properties of a vortex are connected, with a focus on the effects on the lifespans. We first used a vortex extraction algorithm to find all mesoscale vortices that were above given thresholds for size and potential vorticity anomaly at the centre. To do this it was necessary to adjust the PV anomaly field. We then developed a tracking algorithm to follow the vortices through time and link them together across separate data files.

After this, we investigated the following properties of the vortices: tracks, formation and termination points, lifespans, speeds, areas, distances travelled, kinetic energies (and energy densities). We analysed the distributions of these properties across the population and assessed how these properties were related. A clear linear relationship was found between the lifespan of a vortex and the distance it travelled, as would be expected. There was also a clear non-linear relationship between the lifespans and the average speeds, which suggested that there may be an optimal speed (which was close to the mean) which long-lived vortices would travel at.

We contrasted the properties for cyclonic and anticyclonic vortices. We were able to confirm the assertion in [Carton, 2001] that there was a split in the positions of the two types, although there was occasionally vortices which moved to the opposite side of the jet- this was true for anticyclones in particular. The cyclones were found to be larger, while the connection between area and lifespan was more pronounced for the anticyclones. Finally, we saw that anticyclonic vortices lived slightly longer on average.

We then went on to focus on the longest-lived vortices and saw that interactions with other vortices and the jet were somewhat apparent when observing the energy density patterns, and suggested it may be possible to characterize a vortex by this pattern. Finally, we performed linear stability analysis on vortices in different environments and noted that the eigenvalue spectra depended on the situation of the vortex.

A major difficulty that occurred in the course of this project was successfully tracking the vortices. This was true only for the vortices near the jet, confirming that the constant interactions, mergings and splitting processes undergone by the vortices made it exceedingly difficult for the algorithm to distinguish between nearby vortices in order to select the next position. This was somewhat overcome by the introduction of PV anomaly thresholds, which reduced the number of jumps between true vortex tracks. However, a large number of the vortices could not be matched up, which meant that results were skewed by the presence of vortices which supposedly lasted just one day. With more time, ideally the algorithm would be enhanced, perhaps using another threshold such as area, or optimising the choice of limits.

Given accurate tracks, a clearer picture of the connection between properties could be developed. There are also several areas that could be expanded on. In particular, the connection between interactions and lifespan that became apparent in the analysis of the long-lived vortices could be investigated in more detail. Finally, if given considerably more

time, it would be interesting to examine how the stability of different vortices evolves over time (for example, an isolated vortex compared to one which lived the jet), and compare the lifespans and stabilities of the Hetons compared to the other vortices.

9 Appendix

The code used to obtain and sort the vortices for the filtered PV field minus the time-averaged flow is given in sections 9.1 and 9.2. The code used to do this for the inverted field is very similar.

9.1 Obtaining the Vortices

```
1 basinscale_x=3840e5;
2 basinscale_y=3840e5;
3
4 ii=4097;
5 jj=ii;
6
7 hx=basinscale_x/(ii-1);
8 hy=basinscale_y/(jj-1);
9
10 x = 0:hx:basinscale_x;
11 y = 0:hy:basinscale_y;
12
13 [p,q,r,zetav] = read_data2(4097,4097,3, 'qg3_4097_s_av.d');
14
15 bnds = [];
16 b= ones(1,20)/20;
17
18 for i =1:422
19     filename= 'qg3_4097_s.'+string(i)+'.d'
20     if exist(filename,'file')
21         [l,m,n,zet] = read_data2(4097,4097,3,filename);
22         V = zet(:,:,1)- zetav(:,:,1);
23         filtV = filter2(b,V);
24         savename = 'filtV'+string(i)+'.mat'
25         save(savename, 'filtV');
26         bnd = ContourExtraction(flipud(filtV), x,y
27             ',100,1.15,1);
28         bnds = [bnds bnd];
29     end
30 end
31 save('bnds.mat','bnds')
```

9.2 Sorting the Vortices

```
1 %remove vortices of radius ~<50km and PV anomaly at centre
2 <1.5
3 cd('R:\home\pequod_results\3layers\visc_6.25D4__tau0.3\4097
4 x4097_p256_200years__max_spin_100years\4097
5 x4097_p256_200years__max_spin_100years_1')
6
7 bnds = load('Bnds/bnds.mat');
8 bnds = bnds.bnds;
9
10 for count = 1:365
11     disp(count)
12     areas = zeros(1, size(bnds(count).xc, 2));
13     for j = 1:size(bnds(count).xc, 2)
14         xvals = cell2mat(bnds(count).xc(j));
15         yvals = cell2mat(bnds(count).yc(j));
16         areas(j) = polyarea(xvals, yvals);
17     end
18     remove = areas < 14*(10^12);
19     bnds(count).xc(remove) = [];
20     bnds(count).yc(remove) = [];
21     bnds(count).cval(remove) = [];
22     bnds(count).valp(remove) = [];
23     bnds(count).xp(remove) = [];
24     bnds(count).yp(remove) = [];
25
26     valps = zeros(1, size(bnds(count).xc, 2));
27     for j = 1:size(bnds(count).xc, 2)
28         valps(j) = abs(bnds(count).valp(j));
29     end
30
31     remove2 = valps < 1.5;
32     bnds(count).xc(remove2) = [];
33     bnds(count).yc(remove2) = [];
34     bnds(count).cval(remove2) = [];
35     bnds(count).valp(remove2) = [];
36     bnds(count).xp(remove2) = [];
37     bnds(count).yp(remove2) = [];
38 end
```

9.3 Tracking Algorithm

```
1 %get all vortices found by vortex finder for the 365 days
2 bnds3 = load('Bnds/newbnds3.mat','bnds3')
3 bnds3 = bnds3.bnds3;
4
5 firstday = bnds3(1);
6
7 %initialise matrix to store the centres of the vortex
8 %trajectories (one vortex per row, one day per column)
9
10 tracks4 = zeros(size(firstday.xc,2),size(bnds3,2),2);
11
12 %set first column to the (x,y) coordinates of each vortex
13 %from the first day
14 tracks4(:,1,1) = firstday.xp;
15 tracks4(:,1,2) = firstday.yp;
16
17 for i = 1:364
18
19     disp(i)
20     today = tracks4(:,i,:);
21     nextday = [bnds3(i+1).xp',bnds3(i+1).yp',bnds3(i+1).valp
22     '];
23
24     for n = 1:size(today,1)
25         count = 0;
26         coords = [today(n,1,1),today(n,1,2)];
27
28         if coords ~= [0,0]
29             repeat = repmat(coords,size(nextday,1),1);
30             dists = sum((repeat - nextday(:,1:2)).^2,2)
31             .^(1/2);
32             sorted = sort(dists);
33             possible = sorted(1:3);
34             possible = possible(possible < 1.7*10^7);
35
36             if size(possible,1) > 0
37                 distindex = zeros(1,size(possible,2));
38
39                 for j = 1:size(possible,2)
40                     distindex(j) = find(dists == possible(j))
41                     ;
42                 end
43
44             %find today's vortex's max V value
```

```

40         todayindex = find(bnds3(i).xp == coords(1));
41         todayV = bnds3(i).valp(todayindex);
42         disp(todayV)
43
44         diffVs = zeros(1, size(possible, 2));
45
46         for j = 1:size(possible, 2)
47             diffVs(j) = abs(todayV - nextday(
48                 distindex(j), 3));
49         end
50
51         [M, minind] = min(diffVs);
52
53         if M < 0.75 % set this as the position of
54             % the vortex on the next day
55             index = distindex(minind);
56             tracks4(n, i+1, :) = nextday(index, 1:2);
57             count = 1;
58             nextday(index, :) =
59                 [-10^12, -10^12, -10^12]; %to exclude
60                 %, set to value that won't connect with
61                 % any vortices
62         end
63     end
64
65     elseif coords(1) == 0 || count == 0 %if position
66         % of vortex could not be found, try using it's
67         % position the day before
68
69     yestcoords = [tracks4(n, i-1, 1), tracks4(n, i
70         -1, 2)];
71
72     if yestcoords ~= [0,0]
73         repeat2 = repmat(yestcoords, size(nextday, 1)
74             , 1);
75         dists2 = sum((repeat2 - nextday(:, 1:2)).^2, 2)
76             .^(1/2);
77         sorted2 = sort(dists2);
78         possible2 = sorted2(1:3);
79         possible2 = possible2(possible2 < 2.4*10^7);
80
81         if size(possible2, 1) > 0
82             distindex2 = zeros(1, size(possible2, 2));
83
84             for j = 1:size(possible2, 2)

```

```

75         distindex2(j) = find(dists2 ==
76                           possible2(j));
77     end
78
79     %find yesterday's vortex's max V value
80     yestindex = find(bnds3(i-1).xp ==
81                       yestcoords(1));
82     yestV = bnds3(i-1).valp(yestindex);
83     disp('yestV =' +string(yestV))
84
85     diffV2s = zeros(1,size(possible2,2));
86
87     for j = 1:size(possible2,2)
88         diffV2s(j) = abs(yestV - nextday(
89                           distindex2(j),3));
90     end
91
92     [M, minind] = min(diffV2s);
93
94     if M< 1.5
95         index2 = distindex2(minind);
96         tracks4(n, i+1, :) = nextday(index2
97                                         ,1:2);
98         count = 1;
99         nextday(index2,:) =
100             [-10^12,-10^12,-10^12];      %to
101             exclude, set to value that won't
102             connect with any vortices
103             end
104             end
105             end
106             end
107             end
108             end
109             end
110 tracks4(tracks4==0) = NaN;

```

9.4 Properties of the Vortices

9.4.1 Lifespans

```
1 cd('R:\home\pequod_results\3layers\visc_6.25D4_\tau0.3\4097
2     x4097_p256_200years__max_spin_100years\4097
3     x4097_p256_200years__max_spin_100years_1')
4 missing = [];
5 for i =1:422
6     filename = 'filtV/filtV'+string(i)+'.mat';
7     if ~exist(filename)
8         missing=[missing, i];
9     end
10 end
11 lifespans = zeros(1, size(tracks4,1));
12 starts = zeros(1, size(tracks4,1));
13 stops = zeros(1, size(tracks4,1));
14
15 for i = 1:size(tracks4,1)
16     count1 = 0;
17     for j = 1:422
18         if ~ismember(j,missing)
19             count1 = count1 +1;
20             if ~isnan(tracks4(i,count1,1))
21                 start = j;
22                 break
23             end
24         end
25         starts(i) = count1;
26
27         count2 = 366;
28         for j = 422:-1:1
29             if ~ismember(j, missing)
30                 count2 = count2-1;
31                 if ~isnan(tracks4(i,count2,1))
32                     stop = j;
33                     break
34                 end
35             end
36             stops(i) = count2;
37
38             lifespans(i) = stop - start +1;
39 end
```

9.4.2 Terminations and Formations

```
1 formationsall = zeros(size(tracks4,1),2);
2 for i = 1:size(tracks4,1)
3     formationsall(i,:)= tracks4(i,starts(i),:);
4 end
5
6 terminationsall= zeros(size(tracks4,1),2);
7 for i = 1:size(tracks4,1)
8     terminationsall(i,:)= tracks4(i,stops(i),:);
9 end
10
11 formations10plus = zeros(size(lifespans(lifespans >=10),1),2);
12 [rows, cols] = find(lifespans >=10);
13 for i = 1:size(cols,2)
14     formations10plus(i,:)= tracks4(cols(i),starts(cols(i))
15         ,:);
16 end
17 formations40plus = zeros(size(lifespans(lifespans >=40),1),2);
18 [rows, cols] = find(lifespans >=40);
19 for i = 1:size(cols,2)
20     formations40plus(i,:)= tracks4(cols(i),starts(cols(i))
21         ,:);
22 end
23 terminations10plus = zeros(size(lifespans(lifespans >=10),1)
24     ,2);
25 for i = 1:size(cols,2)
26     terminations10plus(i,:)= tracks4(cols(i),stops(cols(i)))
27         ,:);
28 end
29 terminations40plus = zeros(size(lifespans(lifespans >=40),1)
30     ,2);
31 [rows, cols] = find(lifespans >=40);
32 for i = 1:size(cols,2)
33     terminations40plus(i,:)= tracks4(cols(i),stops(cols(i)))
34         ,:);
35 end
```

9.4.3 Areas

```
1 % code to compute the area at each day for each vortex and
2 % the average over
3 % its life
4
5 areas = zeros(size(tracks4, 1), size(tracks4,2));
6 for i = 1:size(tracks4,1)
7     for j = starts(i):stops(i)
8         index = find(bnds3(j).xp == tracks4(i,j,1));
9         xvals = cell2mat(bnds3(j).xc(index));
10        yvals = cell2mat(bnds3(j).yc(index));
11        areas(i,j) = polyarea(xvals, yvals);
12    end
13 end
14 areas(areas == 0) = NaN;
15
16 averageareas = nanmean(areas,2);
```

9.4.4 Speeds and Distances

```
1 speeds2 = zeros(size(tracks4,1),422);
2
3 for i = 1:size(tracks4,1)
4     disp(i)
5     if starts(i) ~= stops(i)
6         truestart = findtrueday(starts(i));
7         truestop = findtrueday(stops(i));
8         filled= zeros(1, (truestop - truestart +1),2);
9         count=starts(i);
10        for j = 1:(truestop-truestart+1)
11            if ~ismember(j,missing)
12                filled(1,j,:)= tracks4(i,count,:);
13                count = count +1;
14            else
15                filled(1,j,:)= [NaN,NaN];
16            end
17        end
18
19        filled = fillmissing(filled, 'linear');
20        for k = 1:(truestop - truestart)
21            speeds2(i,truestart+k) = sqrt(sum((filled(1,k
22                +1,:)-filled(1,k,:)).^2));
```

```

22         end
23     end
24 end
25
26 speeds2(speeds2 == 0) = NaN;
27 totaldists2 = nansum(speeds2,2);
28 avspeeds2 = nanmean(speeds2,2);

```

9.4.5 Energies and Energy Densities

```

1 %cd('R:\home\pequod_results\3layers\visc_6.25D4__tau0.3\4097
2   x4097_p256_200years__max_spin_100years\4097
3   x4097_p256_200years__max_spin_100years_1')
4
5 bnds3 = load('Bnds/newbnds3.mat','bnds3');
6 bnds3 = bnds3.bnds3;
7
8 tracks4 = load('Bnds/finaltracks.mat','tracks4');
9 tracks4 = tracks4.tracks4;
10
11 tops = zeros(1,365);
12 bottoms = zeros(1,365);
13
14 for i = 1:365
15   for j = 1:size(tracks4,1)
16     if ~isnan(tracks4(j,i,1))
17       tops(i) = j;
18       break
19     end
20   end
21 end
22
23 for i = 1:365
24   for j = size(tracks4,1):-1:1
25     if ~isnan(tracks4(j,i,1))
26       bottoms(i) = j;
27       break
28     end
29   end
30 missing = [];
31 for i = 1:422
32   filename = 'filtV/filtV'+string(i)+'.mat';

```

```

33 if ~exist(filename)
34 missing=[missing, i];
35 end
36 end
37
38 layers = 3;
39 ii = 4097;
40 jj = 4097;
41
42 basinscale_x=3840e5;
43 basinscale_y=3840e5; % Physical size of the domain in
44 % centimeters
45 hx=basinscale_x/(ii-1);
46 hy=basinscale_y/(jj-1);
47 [x,y]=meshgrid(0:hx:basinscale_x,basinscale_y:-hy:0);
48
49 energies = zeros(size(tracks4,1),size(tracks4,2));
50
51 [model_time_day_av,total_time_day_av,psi_av,zet_av,omega_av,
52 u_av,v_av]=read_all_data(ii,jj,layers,'qg3/qg3_4097_s_av.d
53 ');
54 u1_av = u_av(:,:,1);
55 v1_av = v_av(:,:,1);
56
57 count = 0;
58 for i = 1:422
59 if ~ismember(i,missing)
60 disp(i)
61 count = count + 1;
62 filename = 'qg3/qg3_4097_s.'+string(i)+'.d';
63 [model_time_day,total_time_day,psi,zet,omega,u,v]=
64 read_all_data(ii,jj,layers,filename);
65
66 u1 = u(:,:,1);
67 u1dash = u1 - u1_av;
68 v1 = v(:,:,1);
69 v1dash = v1 - v1_av;
70
71 rawenergy = 0.5*sqrt(u1dash.^2 + v1dash.^2);
72
73 for j = tops(count):bottoms(count)
74 if ~isnan(tracks4(j,count,1))
75 index = find(bnds3(count).xp == tracks4(j,
76 count,1));
77 xvals = cell2mat(bnds3(count).xc(index));
78 yvals = cell2mat(bnds3(count).yc(index));

```

```
74     is_inside= inpolygon(x,y,xvals,yvals);
75     integral = sum(rawenergy(is_inside));
76     energies(j,count)= integral;
77   end
78 end
79 end
80 end
81
82 energies(energies == 0) = NaN;
83 avenergies = nanmean(energies, 2);
84 energydensities = energies./areas;
85
86 save('energies2.mat','energies');
```

9.5 Cyclonic and Anticyclonic Vortices

```
1 count1 = 0;
2 count2 = 0;
3 for j = 1:size(tracks4,1)
4     for i = 1:365
5         index = find(bnds3(i).xp == tracks4(j,i,1));
6         if bnds3(i).valp(index) < 0
7             count1 = count1 +1;
8             negVs(count1,:,:1) = tracks4(j,:,:1);
9             negVs(count1,:,:2) = tracks4(j,:,:2);
10
11             neglifespans(count1) = lifespans(j);
12
13             negareas(count1,:) = areas(j,:);
14             negaverageareas(count1) = averageareas(j,:);
15
16             negspeeds(count1,:) = speeds(j,:);
17             negaveragespeeds(count1) = avspeeds(j,:);
18
19             negtotaldists(count1) = totaldists(j,:);
20
21             negenergies(count1,:) = energies(j,:);
22             negaverageenergies(count1) = avenergies(j);
23             negenergydensities(count1,:) = energydensities(j
24                                         ,:);
25             negavenergydensities(count1) = avenergydensities(
26                                         j);
27             disp(j)
28             break
29         end
30         if bnds3(i).valp(index) > 0
31             count2 = count2 +1;
32             plusVs(count2,:,:1) = tracks4(j,:,:1);
33             plusVs(count2,:,:2) = tracks4(j,:,:2);
34
35             pluslifespans(count2) = lifespans(j);
36
37             plusareas(count2,:) = areas(j,:);
38             plusaverageareas(count2) = averageareas(j,:);
39
40             plusspeeds(count2,:) = speeds(j,:);
41             plusaveragespeeds(count2) = avspeeds(j,:);
42             plustotaldists(count2) = totaldists(j,:);
```

```

43     plusenergies(count2,:) = energies(j,:);
44     plusaverageenergies(count2) = avenergies(j);
45     plusenergydensities(count2,:) = energydensities(j
46         ,:);
47     plusavenergydensities(count2) = avenergydensities
48         (j);
49     disp(j)
50     break
51 end
52
53 plusall = [pluslifespans',plusaverageareas',plusaveragespeeds
54     ',plusaverageenergies',plusavenergydensities'];
negall = [neglifespans',negaverageareas',negaveragespeeds',
    negaverageenergies',negavenergydensities'];

```

9.6 Other Functions

```
1 function trueday = findtrueday(x)
2
3 cd('R:\home\pequod_results\3layers\visc_6.25D4__tau0.3\4097
4 x4097_p256_200years__max_spin_100years\4097
5 x4097_p256_200years__max_spin_100years_1')
6
7 missing = [];
8 for i =1:422
9     filename = 'filtV/filtV'+string(i)+'.mat';
10    if ~exist(filename)
11        missing=[missing, i];
12    end
13 end
14
15 count =0;
16 for i = 1:422
17     if ~ismember(i,missing)
18         count = count +1;
19     end
20     if count == x
21         trueday = i;
22         break
23     end
24 end
```

References

- [Berloff, 2018] Berloff, P. (2018). Lectures on "introduction to geophysical fluids". http://wwwf.imperial.ac.uk/~pberloff/gfd_lectures.pdf. Accessed: 10-05-2019.
- [Carton, 2001] Carton, X. (2001). Hydrodynamical modeling of oceanic vortices. *Surveys in Geophysics*, 22(3):179–263.
- [Green, 1995] Green, S. I. (1995). *Fluid Vortices*. Kluwer Academic Publishers, Dordrecht, Netherlands.
- [Hadjighasem, 2015] Hadjighasem, A. (2015). Vortex extraction algorithm. <https://github.com/LCSETH/Lagrangian-Averaged-Vorticity-Deviation-LAVD>. Accessed: 20-11-2019.
- [Karabasov et al., 2009] Karabasov, S., Berloff, P. S., and Goloviznin, V. (2009). Cabaret in the ocean gyres. *Ocean Modelling*, 30(2-3):155–168.
- [Shevchenko and Berloff, 2015] Shevchenko, I. and Berloff, P. (2015). Multi-layer quasi-geostrophic ocean dynamics in eddy-resolving regimes. *Ocean Modelling*, 94:1–14.
- [Shevchenko and Berloff, 2017] Shevchenko, I. and Berloff, P. (2017). On the roles of baroclinic modes in eddy-resolving midlatitude ocean dynamics. *Ocean Modelling*, 111:55–65.
- [Vallis, 2006] Vallis, G. K. (2006). *Atmospheric and Oceanic Fluid Dynamics*. Cambridge University Press, Cambridge, U.K.